

Effective Field Theory for Higgs Plus Jet Production

S. Dawson^a, I. M. Lewis^a and Mao Zeng^b

^a*Department of Physics, Brookhaven National Laboratory, Upton, N.Y., 11973, U.S.A.*

^b*C.N. Yang Institute for Theoretical Physics Stony Brook University,
Stony Brook, N.Y., 11794, U.S.A.*

Abstract

We use an effective field theory (EFT) which includes all possible gluon-Higgs dimension-5 and dimension-7 operators to study Higgs boson plus jet production in next-to-leading order QCD. The EFT sheds light on the effect of a finite top quark mass as well as any Beyond-the-Standard Model (BSM) modifications of Higgs-gluon effective couplings. In the gluon channel, the accuracy of the heavy-top approximation for differential distributions arises from the non-interference between the helicity amplitudes of the G^3h and G^2h operators in the $m_h < p_T$ limit at lowest order. One dimension-7 operator involving quark bilinears, however, contributes significantly at high p_T , and potentially offers a channel for seeing BSM effects. One-loop renormalization of these operators is determined, allowing resummation of large logarithms via renormalization group running. NLO numerical results at the LHC are presented, which include $\mathcal{O}(1/m_t^2)$ contributions in the SM limit.

Contents

I. Introduction	3
II. Effective Lagrangian	5
A. Higgs-gluon-quark interaction	5
B. Alternative operator basis	9
C. Gluon self-interaction	10
III. Lowest Order	11
A. Lowest order EFT $q\bar{q}gh$ amplitude	11
B. Lowest Order EFT $gggh$ amplitude	12
C. Squared amplitudes	13
IV. Renormalization of dimension-7 operators	14
V. NLO virtual corrections	16
A. Methods	16
B. One loop $q\bar{q}gh$ amplitudes	17
C. One loop $gggh$ amplitudes	18
D. Soft and Collinear real contributions	19
1. Soft - qg channel	19
2. Final State Collinear - qg channel	20
3. Soft - gg channel	21
4. Final State Collinear - gg channel	21
5. Initial State Collinear - all channels	22
E. Higher-dimensional gluon self interaction contribution	22
VI. NLO real emission helicity amplitudes	23
VII. Phenomenology	26
A. LO results	26
B. Numerical accuracy at NLO	30
C. NLO results	32

VIII. Conclusion	36
Acknowledgments	36
References	37
A. Virtual Contributions	43
B. NLO Real Emission - Quark Amplitudes	44
1. $q\bar{q}ggh$ amplitudes	44
2. $q\bar{q}q\bar{q}$ and $q\bar{q}Q\bar{Q}$ amplitudes	45

I. INTRODUCTION

The recently discovered Higgs boson has all the generic characteristics of a Standard Model Higgs boson and measurements of the production and decay rates agree to the 10 – 20% level with Standard Model (SM) predictions [1–4]. The largest contribution to Standard Model Higgs boson production comes from gluon fusion through a top quark loop and testing the nature of this Higgs-gluon interaction probes the mechanism of electroweak symmetry breaking at high scales. In models with new physics, the gluon fusion rate can be altered by new particles interacting in the loop which contribute to an effective dimension-5 operator [5–7],

$$\mathcal{L}_5 = \hat{C}_1 G^{\mu\nu,A} G_{\mu\nu}^A h. \quad (1)$$

For example, in composite models \hat{C}_1 is changed from its SM value by small contributions of $\mathcal{O}(v^2/f^2)$, where f is a TeV scale parameter corresponding to the composite scale [8–10]. Similarly, supersymmetric models alter the ggh coupling due to the contributions of new particles such as squarks in the loops and also by changes in the Higgs-fermion couplings [3, 4, 11, 12]. The measurement of gluon fusion by itself can only measure a combination of \hat{C}_1 and the top quark Yukawa coupling, but cannot distinguish between the two potential new physics effects [13–15].

The high p_T production of the Higgs boson through the process $pp \rightarrow h + \text{jet}$ is particularly sensitive to new contributions to the Higgs gluon effective coupling [13, 14, 16, 17]. This is straightforward to demonstrate in top partner models where at low energy there is a cancellation between the SM top and the top partner contributions to the gluon fusion

rate for Higgs production, making it extremely difficult to observe top partner physics in this channel [15, 18, 19]. The effects of top partners become apparent, however, when kinematic distributions for 2-particle final states, such as double Higgs production [20, 21], or Higgs plus jet production [22], are analyzed. The measurement of Higgs plus jet production offers the possibility to untangle new physics effects contributing to the Higgs-gluon effective interactions from beyond the SM (BSM) contributions to the Higgs-fermion Yukawa couplings.

The strong Higgs-gluon-light quark interactions can be parameterized through $SU(3)$ invariant effective dimension-5 and dimension-7 operators coupling the Higgs boson to partons, which are well known [23, 24]. The dimension -5 operator of Eq. 1 has been used to calculate SM Higgs production through NNLO [25–27], along with the Higgs p_T distribution [28–30]. At NLO, the total rate can be compared with an analytic result with exact top and bottom quark mass dependence [6], while at NNLO, the effective theory calculation has been compared numerically with the calculation in the full theory [31, 32]. In both instances, the dimension-5 operator gives an extremely accurate approximation to the total rate for Higgs production through gluon fusion. The Lagrangian of Eq. (1) corresponds to the $m_t \rightarrow \infty$ limit of the SM, and \hat{C}_1 has been determined to $\mathcal{O}(\alpha_s^3)$ in the SM [33–36].

In this paper, we examine the effect of both the dimension-5 and dimension -7 gluon-Higgs operators on Higgs plus jet production at NLO QCD. We present analytic formulas which can be applied to arbitrary models of new physics. The effects of these operators on the Higgs p_T distribution has been studied numerically at lowest order in Ref. [24]. The Standard Model rate for Higgs +jet is known analytically at order $\mathcal{O}(\alpha_s^3)$ [37, 38], while the NLO rate is known analytically in the $m_t \rightarrow \infty$ limit, [30, 39, 40] which corresponds to the contribution from \hat{C}_1 . Finite top mass effects in SM NLO corrections have been obtained as a numerical expansion in $1/m_t^2$ [41–44], and agree with the $m_t \rightarrow \infty$ limit only for small Higgs transverse momentum, $p_T \leq 150$ GeV. The electroweak contributions are studied in [45]. The NNLO total cross section in the $m_t \rightarrow \infty$ limit for the gg channel is known [46] while the corresponding results for other partonic channels have been obtained in the threshold approximation [47–49]. For Higgs production in association with more than one jet, exact m_t dependence is known for two and three jets at leading order [50–52], while $m_t \rightarrow \infty$ results are available at NLO for two and three jets [53, 54].

In Section II, we discuss the effective Higgs-gluon effective Lagrangian, and in Section

III we review the lowest order results for Higgs plus jet production in the dimension-7 effective field theory (EFT). The renormalization of the dimension-7 effective Lagrangian coefficients is discussed in Section IV. Sections V and VI contain analytic results for Higgs plus jet production at NLO using the dimension-5 and dimension-7 contributions to the EFT, with the real emission corrections presented as helicity amplitudes using the conventions in [55, 56]. The behavior of tree amplitudes in the massless Higgs limit, $m_h^2 < (p_T^2, s, -t, -u)$, is discussed. As a by-product of our calculation, we obtain the $\mathcal{O}(1/m_t^2)$ contributions to the SM rate, modulo the non-logarithmic terms in the NLO matching coefficients in Eqs. (11),(13) which will be derived in a forthcoming work. Numerical results for the LHC are presented in Section VII, and some conclusions given in Section VIII.

II. EFFECTIVE LAGRANGIAN

A. Higgs-gluon-quark interaction

The calculations of Higgs production from gluon fusion are greatly simplified by using an effective Lagrangian where heavy particles, such as the top quark, are integrated out. The $SU(3)$ invariant effective Lagrangian which parameterizes the CP-conserving Higgs -gluon-light quark strong interactions is,

$$\mathcal{L}_{\text{eff}} = \hat{C}_1 O_1 + \frac{1}{\Lambda^2} \sum_{i=2,3,4,5} \hat{C}_i O_i + \mathcal{O}\left(\frac{1}{\Lambda^4}\right). \quad (2)$$

For SM Higgs production, $\Lambda = m_t$ is either the $\overline{\text{MS}}$ running mass or the pole mass, depending on whether the $\overline{\text{MS}}$ scheme or the pole scheme is used to calculate the matching coefficients, \hat{C}_i . For BSM scenarios, Λ is the scale at which BSM physics generates contributions to \hat{C}_i .

At dimension-5, the unique operator is

$$O_1 = G_{\mu\nu}^A G^{\mu\nu,A} h, \quad (3)$$

where $G_{\mu\nu}^A$ is the gluon field strength tensor. We consider only models with a single scalar Higgs boson, although our results can be trivially generalized to the case with multiple scalars. In the SM, the coefficient, \hat{C}_1 , is, to $\mathcal{O}(\alpha_s^2)$ [6, 7],

$$\hat{C}_1(\mu_R)^{\text{SM}, \overline{\text{MS}}} = \frac{\alpha_s(\mu_R)}{12\pi v} \left\{ 1 + \frac{\alpha_s(\mu_R)}{4\pi} \left[5C_A - 3C_F \right] \right\}, \quad (4)$$

where $C_A = N_c = 3$, $C_F = \frac{N_c^2 - 1}{2N_c} = \frac{4}{3}$, $v = 246$ GeV, and μ_R is an arbitrary renormalization scale of $\mathcal{O}(m_h)$.

The dimension-7 operators, needed for gluon fusion production of Higgs, are [23, 24, 57],

$$O_2 = D_\sigma G_{\mu\nu}^A D^\sigma G^{A,\mu\nu} h \quad (5)$$

$$O_3 = f_{ABC} G_\nu^{A,\mu} G_\sigma^{B,\nu} G_\mu^{C,\sigma} h \quad (6)$$

$$O_4 = g_s^2 \sum_{i,j=1}^{n_{lf}} \bar{\psi}_i \gamma_\mu T^A \psi_i \bar{\psi}_j \gamma^\mu T^A \psi_j h \quad (7)$$

$$O_5 = g_s \sum_{i=1}^{n_{lf}} G_{\mu\nu}^A D^\mu \bar{\psi}_i \gamma^\nu T^A \psi_i h, \quad (8)$$

where our convention for the covariant derivative is $D^\sigma = \partial^\sigma - i g_s T^A G^{A,\sigma}$, $Tr(T^A T^B) = \frac{1}{2} \delta_{AB}$ and $n_{lf} = 5$ is the number of light fermions. The operators O_1 , O_2 and O_3 are the only ones that are needed in pure QCD ($n_{lf} = 0$). In the presence of light quarks, we also need O_4 and O_5 which are related by the equations of motion (eom) to gluon-Higgs operators¹

$$\begin{aligned} O_4 |_{eom} &\rightarrow D^\sigma G_{\sigma\nu}^A D_\rho G^{A,\rho\nu} h \equiv O'_4 \\ O_5 |_{eom} &\rightarrow G_{\sigma\nu}^A D^\nu D^\rho G_\rho^{A,\sigma} h \equiv O'_5. \end{aligned} \quad (9)$$

Since O_4 involves 4 light fermions, the operator contributes to Higgs plus jet production only starting at NLO, in the real-emission processes involving two incoming fermions and two outgoing fermions.

The SM coefficient, \hat{C}_2^{SM} , can be found from the leading $\frac{1}{m_t^2}$ terms in the NLO calculation of $gg \rightarrow h$ [58], in the \overline{MS} scheme,

$$\hat{C}_2^{\text{SM},\overline{MS}}(\mu_R) = -\frac{7\alpha_s(\mu_R)}{720\pi v} \left\{ 1 + \frac{\alpha_s(\mu_R)}{\pi} \left[\frac{29}{84} C_A + \frac{19}{21} C_F + \frac{3}{2} C_F \ln\left(\frac{m_t^2}{\mu_R^2}\right) \right] \right\}. \quad (10)$$

For the remaining SM coefficients, we present only the LO contributions along with the $\alpha_s \ln(m_t^2/\mu_R^2)$ contributions which can be deduced from the renormalization group equations

¹ In our study, only gluons directly interact with the Higgs via a top quark loop or some BSM heavy particle, while quark-Higgs coupling is mediated by gluons.

in Section IV.²

$$\hat{C}_3^{\text{SM},\overline{\text{MS}}}(\mu_R) = \frac{g_s(\mu_R)\alpha_s(\mu_R)}{60\pi v} \left\{ 1 + \frac{\alpha_s(\mu_R)}{\pi} \left[\hat{C}_3^{(1)} + \left(\frac{1}{4}C_A + \frac{3}{2}C_F \right) \ln\left(\frac{m_t^2}{\mu_R^2}\right) \right] \right\} \quad (11)$$

$$\hat{C}_4^{\text{SM},\overline{\text{MS}}}(\mu_R) = \frac{\alpha_s(\mu_R)}{360\pi v} + \mathcal{O}(\alpha_s^2(\mu_R)) \quad (12)$$

$$\hat{C}_5^{\text{SM},\overline{\text{MS}}}(\mu_R) = \frac{\alpha_s(\mu_R)}{20\pi v} \left\{ 1 + \frac{\alpha_s(\mu_R)}{\pi} \left[\hat{C}_5^{(1)} + \left(-\frac{121}{216}C_A + \frac{59}{54}C_F \right) \ln\left(\frac{m_t^2}{\mu_R^2}\right) \right] \right\}. \quad (13)$$

Because the O_4 contribution starts at NLO for Higgs plus jet production, we have only presented the LO value for \hat{C}_4 . Since the above matching coefficients are presented in the $\overline{\text{MS}}$ scheme, the top mass m_t in Eq. (11)-(13), as well as in Eq. (2), should be taken as the $\overline{\text{MS}}$ running top mass evaluated at the renormalization scale μ_R .

To use the μ_R -independent constant parameter $1/(m_t^{\text{pole}})^2$ as the EFT power expansion parameter in Eq. (2), in line with the usual language for EFTs, we substitute into Eq. (2) the relation [60],

$$m_t^{\overline{\text{MS}}}(\mu_R) = m_t^{\text{pole}} \left\{ 1 - \frac{C_F\alpha_s(\mu_R)}{\pi} \left[1 - \frac{3}{4} \ln\left(\frac{m_t^2}{\mu_R^2}\right) \right] + \mathcal{O}(\alpha_s^2) \right\}, \quad (14)$$

which gives,

$$\hat{C}_1^{\text{SM,pole}}(\mu_R) = \hat{C}_1^{\text{SM},\overline{\text{MS}}}(\mu_R), \quad (15)$$

$$\hat{C}_2^{\text{SM,pole}}(\mu_R) = -\frac{7\alpha_s(\mu_R)}{720\pi v} \left\{ 1 + \frac{\alpha_s(\mu_R)}{\pi} \left[\frac{29}{84}C_A + \frac{61}{21}C_F \right] \right\}, \quad (16)$$

$$\hat{C}_3^{\text{SM,pole}}(\mu_R) = \frac{g_s(\mu_R)\alpha_s(\mu_R)}{60\pi v} \left\{ 1 + \frac{\alpha_s(\mu_R)}{\pi} \left[\hat{C}_3^{(1)} + 2C_F + \frac{1}{4}C_A \ln\left(\frac{m_t^2}{\mu_R^2}\right) \right] \right\} \quad (17)$$

$$\hat{C}_4^{\text{SM,pole}}(\mu_R) = \frac{\alpha_s(\mu_R)}{360\pi v} + \mathcal{O}(\alpha_s^2(\mu_R)) \quad (18)$$

$$\hat{C}_5^{\text{SM,pole}}(\mu_R) = \frac{\alpha_s(\mu_R)}{20\pi v} \left\{ 1 + \frac{\alpha_s(\mu_R)}{\pi} \left[\hat{C}_5^{(1)} + 2C_F + \left(-\frac{121}{216}C_A - \frac{11}{27}C_F \right) \ln\left(\frac{m_t^2}{\mu_R^2}\right) \right] \right\}. \quad (19)$$

² The SM matching coefficients are given in Ref. [23], but we found discrepancies at NLO. The $C_A \ln(m_t^2/\mu_R^2)$ terms in our results are one half the values in [23]. Our results are consistent with the O_3 anomalous dimension found in [59] and the O_5 anomalous dimension we calculate in Section IV. The non-logarithmic terms in the NLO matching coefficients, $\hat{C}_3^{(1)}$ and $\hat{C}_5^{(1)}$, will be discussed in a forthcoming work. In this study we will set $\hat{C}_3^{(1)}$ and $\hat{C}_5^{(1)}$ to zero. Also, in Ref. [23] the matching is done off-shell, so the operator equivalence relation of Eq. (9) cannot be used. As a result, in our convention the NLO value for \hat{C}_5 is different. The LO coefficients are in agreement with Refs. [23, 24], once the differing sign conventions are accounted for.

The Feynman rules corresponding to Eq. 2 can be found in a straightforward manner. For most of our calculations, we will use the pure-gluon operators O'_4 and O'_5 in Eq. (9) instead of O_4 and O_5 in Eqs. (7) and (8), so that the Feynman diagrams for Higgs plus jet production from the dimension-7 operators are identical to those from the dimension-5 operator O_1 . The O_3 vertices involve at least 3 gluons, while 2 gluons suffice for the other operators.

There are 2 possible tensor structures [61] for the off-shell $g^{A,\mu}(p_1)g^{B,\nu}(p_2)h(p_3)$ vertex,

$$\begin{aligned} T_1^{\mu\nu} &\equiv g^{\mu\nu}p_1 \cdot p_2 - p_1^\nu p_2^\mu \\ T_2^{\mu\nu} &\equiv p_1^\mu p_2^\nu - p_2^\mu p_2^\nu \frac{p_1^2}{p_1 \cdot p_2} - p_1^\mu p_1^\nu \frac{p_2^2}{p_1 \cdot p_2} + p_1^\nu p_2^\mu \frac{p_1^2 p_2^2}{(p_1 \cdot p_2)^2}. \end{aligned} \quad (20)$$

The Lagrangian of Eq. 2 has the off-shell Feynman rule,

$$\begin{aligned} ggh : & \quad -i\delta_{AB} \left[T_1^{\mu\nu} X_1(p_1, p_2) + T_2^{\mu\nu} X_2(p_1, p_2) \right] \\ X_1(p_1, p_2) &= \left\{ 4\hat{C}_1 - \frac{\hat{C}_2}{\Lambda^2} 4p_1 \cdot p_2 - \frac{\hat{C}_4}{\Lambda^2} \left(\frac{2p_1^2 p_2^2}{p_1 \cdot p_2} \right) + \frac{\hat{C}_5}{\Lambda^2} (p_1^2 + p_2^2) \right\} \\ X_2(p_1, p_2) &= -2p_1 \cdot p_2 \frac{\hat{C}_4}{\Lambda^2}. \end{aligned} \quad (21)$$

The Feynman rules for the off-shell $g(p_1^{A,\mu})g(p_2^{\nu,B})g(p_3^{\rho,C})h(p_4)$ vertex (with all momenta outgoing) are,³

$$\begin{aligned} O_1 : & \quad -4\hat{C}_1 g_s f_{ABC} \left\{ -g^{\mu\nu}(p_1 - p_2)^\rho + g^{\mu\rho}(p_1 - p_3)^\nu + g^{\nu\rho}(p_3 - p_2)^\mu \right\} \\ O_2 : & \quad -4\frac{\hat{C}_2}{\Lambda^2} g_s f_{ABC} \left\{ \mathcal{A}^{\mu\nu\rho}(p_1, p_2, p_3) + \mathcal{A}^{\nu\rho\mu}(p_2, p_3, p_1) + \mathcal{A}^{\rho\mu\nu}(p_3, p_1, p_2) \right\} \\ O_3 : & \quad -6\frac{\hat{C}_3}{\Lambda^2} f_{ABC} Y_0^{\mu\nu\rho}(p_1, p_2, p_3) \\ O_5 : & \quad -g_s \frac{\hat{C}_5}{\Lambda^2} \left\{ f_{ABC} \left[-g^{\mu\nu} p_1^\rho \left(p_1^2 + p_2^2 + p_3^2 - 2p_1 \cdot p_2 - 4p_2 \cdot p_3 \right) \right. \right. \\ & \quad \left. \left. + 2p_1^\nu p_2^\rho p_3^\mu + p_1^\nu p_1^\rho p_3^\mu - p_2^\mu p_2^\rho p_3^\nu \right] + 5 \text{ permutations} \right\}, \end{aligned} \quad (22)$$

³ We omit the \hat{C}_4 ggh vertex because this vertex does not contribute to Higgs +jet at NLO.

where

$$\begin{aligned}
Y_0^{\mu\nu\rho}(p_1, p_2, p_3) &= (p_1^\nu g^{\rho\mu} - p_1^\rho g^{\mu\nu}) p_2 \cdot p_3 + (p_2^\rho g^{\mu\nu} - p_2^\mu g^{\nu\rho}) p_1 \cdot p_3 \\
&\quad + (p_3^\mu g^{\nu\rho} - p_3^\nu g^{\rho\mu}) p_1 \cdot p_2 + p_2^\mu p_3^\nu p_1^\rho - p_3^\mu p_1^\nu p_2^\rho \\
\mathcal{A}^{\mu\nu\rho}(p_1, p_2, p_3) &= (p_1 - p_2)^\rho T_1^{\mu\nu}(p_1, p_2) + p_1 \cdot p_2 \left[X_0^{\mu\nu\rho}(p_1) - X_0^{\nu\mu\rho}(p_2) \right] \\
X_0^{\mu\nu\rho}(p) &= g^{\mu\nu} p^\rho - g^{\mu\rho} p^\nu.
\end{aligned} \tag{23}$$

B. Alternative operator basis

In the previous section, we used the basis of Eqs. (5)-(8) to describe the dimension-7 operators. Here we define another dimension-7 operator,

$$O_6 = -D^\rho D_\rho (G_{\mu\nu}^A G^{\mu\nu,A}) h = m_h^2 O_1, \tag{24}$$

where the last equal sign is only valid for on-shell Higgs production, which will be assumed for the rest of this section. Using the Jacobi identities, without using the equations of motion, we have the operator identity

$$O_6 = m_h^2 O_1 = -2O_2 + 4g_s O_3 + 4O_5. \tag{25}$$

Therefore, we can choose $O_6 = m_h^2 O_1$, O_3 , O_4 , and O_5 as a complete basis for the dimension-7 Higgs-gluon-light quark operators. We can rewrite Eq. (2) as

$$\mathcal{L}_{\text{eff}} = C_1 O_1 + \frac{1}{\Lambda^2} (C_3 O_3 + C_4 O_4 + C_5 O_5), \tag{26}$$

where the re-defined matching coefficients are related to those in Eqs. (4),(10)-(13), (15)-(19) by,

$$C_1 \equiv \hat{C}_1 - \frac{m_h^2}{2\Lambda^2} \hat{C}_2, \tag{27}$$

$$C_3 \equiv 2g_s \hat{C}_2 + \hat{C}_3, \tag{28}$$

$$C_4 \equiv \hat{C}_4, \tag{29}$$

$$C_5 \equiv 2\hat{C}_2 + \hat{C}_5. \tag{30}$$

We will use the basis of Eq. 26 for our phenomenological studies.

In particular, for SM Higgs production, using $m_t = m_t^{\text{pole}}$ in Eq. (26), we have

$$C_1^{\text{SM,pole}}(\mu_R) = \frac{\alpha_s(\mu_R)}{12\pi v} \left\{ 1 + \frac{\alpha_s(\mu_R)}{4\pi} [5C_A - 3C_F] \right\} + \frac{7\alpha_s(\mu_R)m_h^2}{1440\pi v m_t^2} \left\{ 1 + \frac{\alpha_s(\mu_R)}{\pi} \left[\frac{29}{84}C_A + \frac{19}{21}C_F + \frac{3}{2}C_F \ln \left(\frac{m_t^2}{\mu_R^2} \right) \right] \right\}, \quad (31)$$

$$C_3^{\text{SM,pole}}(\mu_R) = -\frac{g_s(\mu_R)\alpha_s(\mu_R)}{360\pi v} \left\{ 1 + \frac{\alpha_s(\mu_R)}{\pi} \left[\frac{29}{12}C_A + \frac{25}{3}C_F - 6\hat{C}_3^{(1)} - \frac{3}{2}C_A \ln \left(\frac{m_t^2}{\mu_R^2} \right) \right] \right\}, \quad (32)$$

$$C_4^{\text{SM,pole}}(\mu_R) = \frac{\alpha_s(\mu_R)}{360\pi v} + \mathcal{O}(\alpha_s^2(\mu_R)), \quad (33)$$

$$C_5^{\text{SM,pole}}(\mu_R) = \frac{11\alpha_s(\mu_R)}{360\pi v} \left\{ 1 + \frac{\alpha_s(\mu_R)}{\pi} \left[-\frac{29}{132}C_A + \frac{47}{33}C_F + \frac{18}{11}\hat{C}_5^{(1)} + \left(-\frac{11}{12}C_A - \frac{2}{3}C_F \right) \ln \left(\frac{m_t^2}{\mu_R^2} \right) \right] \right\}. \quad (34)$$

For the $gg \rightarrow h$ amplitude, O_3 , O_4 , and O_5 give vanishing contributions at both tree level and the one-loop level, due either to the lack of quark propagator lines or to the lack of a scale in the diagrams. This leaves us with the operator O_1 multiplied by the matching coefficient C_1 in Eq. (31) which is defined to include $\mathcal{O}(m_h^2/m_t^2)$ terms. This is essentially equivalent to calculating in the $m_t \rightarrow \infty$ limit and applying a rescaling factor. For Higgs plus jet production, though, the other operators will come into play and impact differential distributions.

C. Gluon self-interaction

At $\mathcal{O}(1/m_t^2)$ in the SM, we also need the dimension-6 gluon self-interaction Lagrangian which arises from integrating out the top quark and performing Collins-Wilczek-Zee zero-momentum subtraction to obtain decoupling of the heavy top [62],

$$\begin{aligned} \mathcal{L}_{\text{eff}}^{\text{SM,self}} &= \frac{1}{m_t^2} \left(\frac{g_s\alpha_s}{720\pi} f_{ABC} G_\nu^{A,\mu} G_\sigma^{B,\nu} G_\mu^{C,\sigma} - \frac{\alpha_s}{60\pi} D^\sigma G_{\sigma\nu}^A D_\rho G^{A,\rho\nu} \right), \\ &\equiv \frac{1}{m_t^2} \left(\frac{g_s\alpha_s}{720\pi} \tilde{O}_3 - \frac{\alpha_s}{60\pi} \tilde{O}_4 \right), \end{aligned} \quad (35)$$

where the \tilde{O}_i 's are defined to be identical to the O_i 's in Eq. (5)-(8), but with the Higgs field, h , stripped from the operator definition. Here the matching coefficients are only given at leading order because this is sufficient for NLO Higgs plus jet production.

There is a neat way to obtain the above effective Lagrangian. Using the Higgs low-energy theorems [5], it is easy to see that at leading order matching, the $\mathcal{O}(1/m_t^2)$ terms in Eq. (2) and (35) can be packaged together in the expression,

$$\mathcal{L}^{\text{SM}}|_{\mathcal{O}(1/m_t^2)} = -\frac{v}{2m_t^2 \left(1 + \frac{h}{v}\right)^2} \sum_{i=2,3,4,5} \hat{C}_i \tilde{O}_i. \quad (36)$$

Starting from Eq. (36), we use the operator relation of Eq. (25) (which can be applied to \tilde{O}_i 's instead of O_i 's by setting $m_h = 0$) to eliminate \tilde{O}_2 , and further use the relation $\tilde{O}_4 = \tilde{O}_5$, valid only at zero-momentum, to eliminate \tilde{O}_5 , to reach Eq. (35) which only involves \tilde{O}_3 and \tilde{O}_4 . In a BSM model, the coefficients of the gluon self-interactions depend on the nature of the heavy physics which is integrated out.

III. LOWEST ORDER

The lowest order amplitudes for Higgs + jet production including all fermion mass dependence (bottom and top) are given in Refs. [37, 38]. The effective Lagrangian can be used to obtain the contributions from the top quark in the infinite mass approximation, along with the SM results including terms of $\mathcal{O}(1/m_t^2)$. At the lowest order in α_s , O_3 is the only dimension-7 operator which contributes to the $gg \rightarrow gh$ channel, while O_5 is the only dimension-7 operator which contributes to channels with initial state quarks.

A. Lowest order EFT $q\bar{q}gh$ amplitude

There are 2 independent gauge invariant tensor structures for the process $0 \rightarrow q\bar{q}hg$, (where we consider all momenta outgoing) [63, 64]

$$\mathcal{T}_1^\mu \equiv i \left(p_{\bar{q}}^\mu \bar{u}(p_q) \not{p}_g v(p_{\bar{q}}) - \frac{S_{g\bar{q}}}{2} \bar{u}(p_q) \gamma^\mu v(p_{\bar{q}}) \right) \quad (37)$$

$$\mathcal{T}_2^\mu = i \left(p_q^\mu \bar{u}(p_q) \not{p}_g v(p_{\bar{q}}) - \frac{S_{gq}}{2} \bar{u}(p_q) \gamma^\mu v(p_{\bar{q}}) \right), \quad (38)$$

where $S_{q\bar{q}} = (p_q + p_{\bar{q}})^2$, $S_{gq} = (p_g + p_q)^2$, and $S_{g\bar{q}} = (p_g + p_{\bar{q}})^2$. The $0 \rightarrow q\bar{q}gh$ amplitude is given in general by,

$$M_{q\bar{q}gh}^{\alpha,\mu} = \sum_{i=1,3-5} T^A \left(B_1^{\alpha,i} \mathcal{T}_1^\mu + B_2^{\alpha,i} \mathcal{T}_2^\mu \right), \quad (39)$$

where $\alpha = 0, 1$ denotes the order of the calculation (LO, NLO), and the sum is over the contributions of the different operators. The tree level amplitude to $\mathcal{O}(1/\Lambda^2)$ is,

$$M_{qqgh}^{0,\mu} = T^A(\mathcal{T}_1^\mu + \mathcal{T}_2^\mu) \left[C_1 \left(\frac{-4g_s}{S_{q\bar{q}}} \right) + \frac{C_5}{\Lambda^2}(-g_s) \right], \quad (40)$$

i.e., the non-vanishing coefficients in Eq. 39 are,

$$\begin{aligned} B_1^{0,1} &= B_2^{0,1} = C_1 \left(\frac{-4g_s}{S_{q\bar{q}}} \right) \\ B_1^{0,5} &= B_2^{0,5} = \frac{C_5}{\Lambda^2}(-g_s). \end{aligned} \quad (41)$$

B. Lowest Order EFT $gggh$ amplitude

There are 4 independent gauge invariant tensor structures for the $0 \rightarrow g(p_1^\mu)g(p_2^\nu)g(p_3^\rho)h$ amplitude [37, 63, 64], assuming all momenta outgoing and $S_{ij} = 2p_i \cdot p_j$,

$$\begin{aligned} \mathcal{Y}_0^{\mu\nu\rho}(p_1, p_2, p_3) &= (p_1^\nu g^{\rho\mu} - p_1^\rho g^{\mu\nu}) \frac{S_{23}}{2} + (p_2^\rho g^{\mu\nu} - p_2^\mu g^{\nu\rho}) \frac{S_{31}}{2} \\ &\quad + (p_3^\mu g^{\nu\rho} - p_3^\nu g^{\rho\mu}) \frac{S_{12}}{2} + p_2^\mu p_3^\nu p_1^\rho - p_3^\mu p_1^\nu p_2^\rho \end{aligned} \quad (42)$$

$$\mathcal{Y}_1^{\mu\nu\rho}(p_1, p_2, p_3) = p_2^\mu p_1^\nu p_1^\rho - p_2^\mu p_1^\nu p_2^\rho \frac{S_{31}}{S_{23}} - \frac{1}{2} p_1^\rho g^{\mu\nu} S_{12} + \frac{1}{2} p_2^\rho g^{\mu\nu} \frac{S_{31} S_{12}}{S_{23}} \quad (43)$$

$$\mathcal{Y}_2^{\mu\nu\rho}(p_1, p_2, p_3) = \mathcal{Y}_1^{\rho\mu\nu}(p_3, p_1, p_2)$$

$$\mathcal{Y}_3^{\mu\nu\rho}(p_1, p_2, p_3) = \mathcal{Y}_1^{\nu\rho,\mu}(p_2, p_3, p_1).$$

An arbitrary $gggh$ amplitude is written as

$$\begin{aligned} \mathcal{M}_{gggh}^{\alpha,\mu\nu\rho} &= f_{ABC} \sum_i \left\{ A_0^{\alpha,i}(p_1, p_2, p_3) \mathcal{Y}_0^{\mu\nu\rho}(p_1, p_2, p_3) + \right. \\ &\quad \left. \sum_{m=1,2,3} A_m^{\alpha,i}(p_1, p_2, p_3) \mathcal{Y}_m^{\mu\nu\rho}(p_1, p_2, p_3) \right\}, \end{aligned} \quad (44)$$

where again $\alpha = 0, 1$ for the lowest order (LO) and next-to-leading order (NLO) contributions, i is the contribution corresponding to O_i , and

$$\begin{aligned} A_2^{\alpha,i}(p_1, p_2, p_3) &= A_1^{\alpha,i}(p_3, p_1, p_2) \\ A_3^{\alpha,i}(p_1, p_2, p_3) &= A_1^{\alpha,i}(p_2, p_3, p_1). \end{aligned} \quad (45)$$

The LO contributions from O_1 and O_3 are

$$\begin{aligned}
A_0^{0,1}(p_1, p_2, p_3) &= 8g_s C_1 \left(\frac{1}{S_{12}} + \frac{1}{S_{23}} + \frac{1}{S_{31}} \right) \\
A_1^{0,1}(p_1, p_2, p_3) &= \frac{8g_s C_1}{S_{31}} \\
A_0^{0,3}(p_1, p_2, p_3) &= \frac{C_3}{\Lambda^2} 6 \\
A_1^{0,3}(p_1, p_2, p_3) &= 0,
\end{aligned} \tag{46}$$

while the O_5 contribution vanishes.

C. Squared amplitudes

To obtain squared amplitudes, we need the interference between the Lorentz / Dirac tensor structures, and the interference between the color structures. For the $qg \rightarrow qh$ squared amplitude, the interferences between the tensor structures are (omitting the ones which can be obtained from $q \leftrightarrow \bar{q}$ crossing symmetry between \mathcal{T}_1 and \mathcal{T}_2).

$$\sum_A \text{tr}(\mathbf{T}^A \mathbf{T}^A) = \frac{N_c^2 - 1}{2}, \tag{47}$$

$$-\sum_{\text{spins}} \mathcal{T}_1^\mu \mathcal{T}_{1,\mu}^\dagger = -(1 - \epsilon) S_{q\bar{q}} S_{gq}^2, \tag{48}$$

$$-\sum_{\text{spins}} \mathcal{T}_1^\mu \mathcal{T}_{2,u}^\dagger = -\epsilon S_{q\bar{q}} S_{gq} S_{g\bar{q}}, \tag{49}$$

where external fermion spinors are implicit and we work in $N = 4 - 2\epsilon$ dimensions. The $q\bar{q} \rightarrow gh$ squared amplitude can be obtained from crossing the $qg \rightarrow qh$ squared amplitude. For the $gg \rightarrow gh$ squared amplitude, the interferences between the tensor structures are,

$$\sum_{ABC} f^{ABC} f^{ABC} = N_c(N_c^2 - 1), \tag{50}$$

$$-\sum_{\text{spins}} \mathcal{Y}_0^{\mu\nu\rho} \mathcal{Y}_{0,\mu\nu\rho}^\dagger = \left(1 - \frac{3}{2}\epsilon\right) S_{12} S_{23} S_{31}, \tag{51}$$

$$-\sum_{\text{spins}} \mathcal{Y}_1^{\mu\nu\rho} \mathcal{Y}_{0,\mu\nu\rho}^\dagger = \frac{1}{2}(1 - \epsilon) S_{12}^2 S_{31}, \tag{52}$$

$$-\sum_{\text{spins}} \mathcal{Y}_1^{\mu\nu\rho} \mathcal{Y}_{1,\mu\nu\rho}^\dagger = \frac{1}{2}(1 - \epsilon) \frac{S_{12}^3 S_{31}}{S_{23}}, \tag{53}$$

$$-\sum_{\text{spins}} \mathcal{Y}_1^{\mu\nu\rho} \mathcal{Y}_{2,\mu\nu\rho}^\dagger = \frac{1}{4} S_{12} S_{31}^2, \tag{54}$$

where we have omitted terms which can be obtained from cyclic permutations.

Here we present squared amplitudes, summed (but not averaged) over initial and final state spins, with $\mathcal{O}(\epsilon)$ terms omitted. For $gg \rightarrow gh$, the squared amplitude from the O_1 operator is [37]

$$\sum_{\text{spins}} \left| M_{gg \rightarrow gh, O_1}^{(0)} \right|^2 = 384 C_1^2 \frac{m_h^8 + s^4 + t^4 + u^4}{stu}, \quad (55)$$

while the O_1 - O_3 interference contribution is

$$\sum_{\text{spins}} M_{gg \rightarrow gh, O_1}^{(0)} \cdot M_{gg \rightarrow gh, O_3}^{(0), \dagger} + \text{c.c.} = 1152 C_1 C_3 \frac{m_h^4}{\Lambda^2}. \quad (56)$$

Interestingly, the O_1 contribution, Eq. (55), corresponding to a rescaled $m_t \rightarrow \infty$ approximation, grows as p_T^2 for high p_T Higgs production, while the O_1 - O_3 interference contribution, Eq. (56), remains constant and therefore diminishes in relative importance, in contrary to the generic behavior of higher-dimensional operators. This results in suppressed top mass dependence in Higgs differential distributions in the gluon channel, and will be explained by the helicity structure of the amplitudes in the soft Higgs limit, i.e. the limit $m_h^2 < (p_T^2, s, -t, -u)$, discussed in Section VI.

For $qg \rightarrow qh$, the squared amplitude from the O_1 operator is [37]

$$\sum_{\text{spins}} \left| M_{qg \rightarrow qh, O_1}^{(0)} \right|^2 = 64 C_1^2 \frac{s^2 + u^2}{-t}, \quad (57)$$

while the O_1 - O_5 interference contribution is

$$\sum_{\text{spins}} M_{qg \rightarrow qh, O_1}^{(0)} \cdot M_{qg \rightarrow qh, O_5}^{(0), \dagger} + \text{c.c.} = -32 C_1 C_5 \frac{s^2 + u^2}{\Lambda^2} \quad (58)$$

The results, crossed into the $q\bar{q} \rightarrow gh$ channel, are

$$\sum_{\text{spins}} \left| M_{q\bar{q} \rightarrow gh, O_1}^{(0)} \right|^2 = 64 C_1^2 \frac{t^2 + u^2}{s}, \quad (59)$$

$$\sum_{\text{spins}} M_{q\bar{q} \rightarrow gh, O_1}^{(0)} \cdot M_{q\bar{q} \rightarrow gh, O_5}^{(0), \dagger} + \text{c.c.} = 32 C_1 C_5 \frac{t^2 + u^2}{\Lambda^2}. \quad (60)$$

IV. RENORMALIZATION OF DIMENSION-7 OPERATORS

In this section, we use the basis $O_6 \cong m_h^2 O_1$, O_3 , O_4 , and O_5 , described in Section II.B, for the dimension-7 operators. In addition to the renormalization of the QCD coupling constant

and self energies in both QCD vertices and the O_i operators, we need to renormalize the C_i matching coefficients. The renormalization of C_1 is well known [65–67], and is identical to the renormalization of α_s at one-loop. The renormalization of C_3 and C_5 are different, and they will be presented as the sum of α_s renormalization and an extra piece. The renormalization of C_3 was found in Ref. [59]. The renormalization of C_5 is a new result.

The unrenormalized effective Lagrangian coupling the Standard Model Higgs boson to gluons is,

$$\mathcal{L}_{\text{eff}} = C_1^{\text{bare}} O_1^{\text{bare}} + \sum_{i=3-5} \frac{C_i^{\text{bare}}}{\Lambda^2} O_i^{\text{bare}}, \quad (61)$$

where Λ is a constant power expansion parameter that should not depend on μ_R , so in this section we will allow Λ to be equal to the top quark pole mass in the case of SM Higgs production, but not the running $\overline{\text{MS}}$ mass. The operators O_i^{bare} are defined in the same way as O_i , but with all the fields and couplings replaced by bare quantities. O_4 is needed only at LO, so we will not discuss its one-loop renormalization. In our operator basis, the one-loop mixing matrix is diagonal, so we can write

$$C_i^{\text{bare}} = C_i + \delta C_i = Z_i C_i = (1 + \delta Z_i) C_i. \quad (62)$$

The renormalization constants Z_i are found using two different methods. The first one is to calculate one-loop ggh , $gggh$, and $q\bar{q}gh$ amplitudes on-shell, and impose transverse gluon polarizations to eliminate spurious mixing into gauge non-invariant operators. The second method is to calculate these one-loop amplitudes off-shell to reduce the number of diagrams needed, and use the background field method [68] to preserve gauge-invariance. In either method, the divergences are matched to the tensor structures arising from the various operators in order to extract the renormalization of the C_i . The renormalization counterterms are given by,

$$\delta Z_1 = \delta Z_{\alpha_s}, \quad (63)$$

$$\delta Z_3 = \frac{3}{2} \delta Z_{\alpha_s} + \frac{\alpha_s}{2\pi\epsilon} (4\pi)^\epsilon r_\Gamma 3C_A, \quad (64)$$

$$\delta Z_5 = \delta Z_{\alpha_s} + \frac{\alpha_s}{2\pi\epsilon} (4\pi)^\epsilon r_\Gamma \left(\frac{11}{6} C_A + \frac{4}{3} C_F \right), \quad (65)$$

where r_Γ is given in Eq. (76), and

$$\delta Z_{\alpha_s} = \frac{\alpha_s}{\pi\epsilon} (4\pi)^\epsilon r_\Gamma b_0, \quad (66)$$

$$b_0 = \left(\frac{11}{12} C_A - \frac{1}{6} n_f \right), \quad (67)$$

is the one-loop renormalization factor for the strong coupling α_s in an $n_f = 5$ flavor theory, proportional to the beta function.

By using

$$\frac{d \ln C_i}{d \ln \mu_R} = -\frac{d \ln Z_i}{d \ln \mu_R}, \quad (68)$$

we have the following renormalization group running equations,

$$\frac{d}{d \ln \mu_R} \ln \left(\frac{C_1}{g_s^2} \right) = \mathcal{O}(\alpha_s^2(\mu_R)), \quad (69)$$

$$\frac{d}{d \ln \mu_R} \ln \left(\frac{C_3}{g_s^2} \right) = \frac{\alpha_s(\mu_R)}{\pi} 3C_A, \quad (70)$$

$$\frac{d}{d \ln \mu_R} \ln \left(\frac{C_5}{g_s^2} \right) = \frac{\alpha_s(\mu_R)}{\pi} \left(\frac{11}{6}C_A + \frac{4}{3}C_F \right). \quad (71)$$

The leading-logarithmic solutions to the renormalization group running of Eqs. (69)-(71) are

$$C_1(\mu_R)/g_s^2(\mu_R) = C_1(\mu_0)/g_s^2(\mu_0), \quad (72)$$

$$C_3(\mu_R)/g_s^3(\mu_R) = \left(\frac{\alpha_s(\mu_R)}{\alpha_s(\mu_0)} \right)^{-\frac{3C_A}{2b_0}} \cdot C_3(\mu_0)/g_s^3(\mu_0), \quad (73)$$

$$C_5(\mu_R)/g_s^2(\mu_R) = \left(\frac{\alpha_s(\mu_R)}{\alpha_s(\mu_0)} \right)^{-\frac{1}{2b_0} \left(\frac{11}{6}C_A + \frac{4}{3}C_F \right)} \cdot C_5(\mu_0)/g_s^2(\mu_0), \quad (74)$$

which in principle allows us to perform matching at the new physics scale Λ , and use renormalization group running to obtain C_i at $\mu_R \sim m_h$, hence resumming large logarithms of Λ/m_h .

V. NLO VIRTUAL CORRECTIONS

A. Methods

All our NLO calculations are done using O_1 , O_3 , and O_5 as a basis of operators, as described in Section II B, with $O(m_h^2/m_t^2)$ terms included in the C_1 matching coefficient to absorb the dimension-7 operator O_6 operator in Eq. (24). When calculating NLO virtual amplitudes for O_5 , we exploit equations of motions to use the O'_5 operator in Eq. (9) instead. The NLO virtual diagrams needed for O_1 are also the only ones needed for O_3 and O'_5 . Our amplitude-level results, given as coefficients for the tensor structures in Eqs. (37),(38),(42)-(44), are valid in both the conventional dimensional regularization (CDR) scheme in D

dimensions and the t'Hooft-Veltman scheme which has loop momenta in D dimensions and external leg momenta in 4 dimensions.

The one-loop virtual calculation is done as follows. The software FeynRules [69] is used to generate Feynman rules for each of the operators. FeynArts [70] is used to generate Feynman diagrams and produce expressions for the amplitudes by using the Feynman rules, with loop integrations unperformed. FormCalc [71] is used to perform the numerator algebra and loop integration, producing results in terms of one-loop tensor integrals (up to rank-5 box integrals). The tensor integrals are subsequently reduced to scalar integrals in D dimensions using FeynCalc [72], and combined with the explicit results for the scalar integrals [73] to produce our final analytic results for the one-loop virtual amplitudes. Alternatively, the tensor integrals can be evaluated numerically using LoopTools [71] without analytic reduction to scalar integrals, and we have checked that the results agree numerically with our analytic formulas for the one-loop amplitudes.⁴

B. One loop $q\bar{q}gh$ amplitudes

The one-loop virtual amplitudes for $0 \rightarrow q\bar{q}gh$ and the real emission amplitudes for $0 \rightarrow q\bar{q}ggh$ are responsible for both $qg \rightarrow h + j + X$ and the $q\bar{q} \rightarrow h + j + X$, where $j = g, q$ or \bar{q} .

We list only the B_2 contributions for the virtual one-loop diagrams from each of the operators since B_1 can be obtained by exchanging S_{gq} and $S_{g\bar{q}}$. The virtual contribution proportional to C_4 vanishes.

The non-vanishing one-loop coefficients, $B_2^{1,i}$ defined in Eq. 39, from the operators O_i are,

$$\begin{aligned}
 B_2^{1,1} &= \frac{\alpha_s(\mu_R)}{4\pi} r_\Gamma \left(\frac{4\pi\mu_R^2}{m_h^2} \right)^\epsilon B_2^{0,1} \left[N_c V_1 + \frac{1}{N_c} V_2 + n_{lf} V_3 \right] \\
 B_2^{1,3} &= \frac{C_3}{m_t^2} \frac{\alpha_s(\mu_R)}{8\pi} N_c \\
 B_2^{1,5} &= \frac{\alpha_s(\mu_R)}{4\pi} r_\Gamma \left(\frac{4\pi\mu^2}{m_h^2} \right)^\epsilon B_2^{0,5} \left[N_c W_1 + \frac{1}{N_c} W_2 + n_{lf} W_3 \right], \tag{75}
 \end{aligned}$$

⁴ We find that there are some special tensor integrals which cannot be reduced to scalar integrals correctly by FeynCalc in D dimensions, but this problem has not affected our calculation, since the end results are in agreement with LoopTools.

where

$$r_\Gamma \equiv \frac{\Gamma^2(1-\epsilon)\Gamma(1+\epsilon)}{\Gamma(1-2\epsilon)}. \quad (76)$$

Analytic expressions for the functions V_i and W_i are given in Appendix A.

The $0 \rightarrow q\bar{q}gh$ amplitude involves one ordinary QCD coupling and one EFT coupling, both of which need counterterms. The sum of the counterterms is

$$M_{q\bar{q}gh}^{CT,\mu} = \frac{3}{2}\delta Z_{\alpha_s} M_{q\bar{q}gh}^{0,\mu} - g_s(\mu_R) T^A (\mathcal{T}_1 + \mathcal{T}_2)^\mu \frac{\alpha_s(\mu_R)}{2\pi\epsilon} \left(\frac{11}{6} C_A + \frac{4}{3} C_F \right) \frac{C_5}{\Lambda^2}, \quad (77)$$

where the renormalization for the O_1 amplitude is simply proportional to 3 times the g_s renormalization [30, 74], whereas there is an extra term for the O_5 amplitude because the C_5 renormalization in Eq. (65) is not proportional to δZ_{α_s} .

The renormalized one-loop virtual amplitude is then,

$$M_{q\bar{q}gh}^{V+CT,\mu} = \left(\frac{4\pi\mu_R^2}{m_h^2} \right)^\epsilon r_\Gamma \left\{ \left[\frac{A_{V2}}{\epsilon^2} + \frac{A_{V1}}{\epsilon} \right] M_{q\bar{q}gh}^\mu + \left(\mathcal{T}_1 + \mathcal{T}_2 \right)^\mu T^A A_{V0} \right\}, \quad (78)$$

where

$$\begin{aligned} A_{V2} &= \frac{\alpha_s(\mu_R)}{4\pi} \left(-2N_c + \frac{1}{N_c} \right) \\ A_{V1} &= \frac{\alpha_s(\mu_R)}{4\pi} \left\{ N_c \ln \left(\frac{-S_{gq}}{m_h^2} \right) + N_c \ln \left(\frac{-S_{g\bar{q}}}{m_h^2} \right) - \frac{1}{N_c} \ln \left(\frac{-S_{q\bar{q}}}{m_h^2} \right) \right\}. \end{aligned} \quad (79)$$

Note that the finite contribution to the virtual amplitude, A_{V0} , is not proportional to the LO result. A_{V0} is just the contribution from the finite terms in defined in Eq. 75 and Appendix A.

C. One loop $gggh$ amplitudes

The 1-loop virtual results are,

$$\begin{aligned} A_0^{1,1} &= \frac{\alpha_s(\mu_R)}{4\pi} r_\Gamma \left(\frac{4\pi\mu^2}{m_h^2} \right)^\epsilon N_c U_1 A_0^{0,1} \\ A_1^{1,1} &= \frac{\alpha_s(\mu_R)}{4\pi} r_\Gamma \left(\frac{4\pi\mu^2}{m_h^2} \right)^\epsilon \left[N_c U_1 A_1^{0,1} + \frac{8g_s(N_c - N_{lf}) S_{23}}{3S_{12}^2} \right] \\ A_0^{1,3} &= \frac{\alpha_s(\mu_R)}{4\pi} r_\Gamma \left(\frac{4\pi\mu^2}{m_h^2} \right)^\epsilon N_c U_3 A_0^{0,3} \\ A_1^{1,3} &= 0 \\ A_0^{1,5} &= 0 \\ A_1^{1,5} &= -\frac{g_s\alpha_s(\mu_R)}{4\pi} \cdot \frac{2S_{23}}{3S_{12}}. \end{aligned} \quad (80)$$

Analytic expressions for the functions U_1 and U_3 are given in Appendix A.

The counterterm from renormalization for the QCD coupling and the EFT matching coefficients is,

$$\begin{aligned}
\mathcal{M}_{ggh}^{CT,\mu\nu\rho} = f_{ABC} & \left\{ \left(\delta Z_1 + \frac{1}{2} \delta Z_{\alpha_s} \right) \left(A_0^{0,1}(p_1, p_2, p_3) \mathcal{Y}_0^{\mu\nu\rho}(p_1, p_2, p_3) + \right. \right. \\
& \sum_{m=1,2,3} A_m^{0,1}(p_1, p_2, p_3) \mathcal{Y}_m^{\mu\nu\rho}(p_1, p_2, p_3) \left. \right) \\
& + \delta Z_3 \left(A_0^{0,3}(p_1, p_2, p_3) \mathcal{Y}_0^{\mu\nu\rho}(p_1, p_2, p_3) + \right. \\
& \left. \left. \sum_{m=1,2,3} A_m^{0,3}(p_1, p_2, p_3) \mathcal{Y}_m^{\mu\nu\rho}(p_1, p_2, p_3) \right) \right\} \quad (81)
\end{aligned}$$

D. Soft and Collinear real contributions

1. Soft - qg channel

We combine the virtual and real amplitudes using the 2 cut-off phase space slicing method to regulate the soft and collinear singularities in D dimensions [75] for the $qg \rightarrow h + j + X$ and $gg \rightarrow h + j + X$ channels. The results for $q\bar{q} \rightarrow h + j + X$ can be obtained in a similar manner and are included in our numerical results.

To find the NLO cross section, we integrate the LO, NLO virtual, soft and collinear contributions over the 2-body final state phase space, and integrate the hard non-collinear contribution over the 3-body final phase space. The total answer is finite and independent of δ_c and δ_s .

The soft contribution is defined as the contribution from real gluon emission, $qg \rightarrow qgh$, where the outgoing gluon has an energy less than a small cut-off [75],

$$E_g < \delta_s \frac{\sqrt{s}}{2}. \quad (82)$$

where δ_s is an arbitrary small number. For the qg initial state, $s = S_{g\bar{q}}$, $t = S_{q\bar{q}}$, and $u = S_{qq}$.

The soft contribution is found by integrating the eikonal approximation to the $qg \rightarrow qh + g_{\text{soft}}$ amplitude-squared and integrating over the soft gluon phase space following exactly the procedure of Ref. [75]. The required integrals are found in Ref. [76]. The soft result is,

$$|M_{qg \rightarrow qh}^{\text{soft}}|^2 = -\frac{\alpha_s(\mu_R)}{4\pi} r_\Gamma \left(\frac{4\pi\mu_R^2}{m_h^2} \right)^\epsilon |M_{qg \rightarrow qh}^{(0)}|^2 \left\{ A_{2S} \frac{1}{\epsilon^2} + A_{1S} \frac{1}{\epsilon} + A_{0S} \right\}, \quad (83)$$

where,

$$\begin{aligned}
A_{S2} &= -\frac{34}{3}, \\
A_{S1} &= \frac{68}{3} \ln \delta_s - 6 \ln \left(\frac{m_h^2 \beta_H}{-u} \right) - 6 \ln \left(\frac{m_h^2}{s} \right) + \frac{2}{3} \ln \left(\frac{m_h^2 \beta_H}{-t} \right) \\
&\quad - \ln \left(\frac{s}{m_h^2} \right) A_{S2} \\
A_{S0} &= -\frac{68}{3} \ln^2 \delta_s + 12 \left(\ln \frac{m_h^2 \beta_h}{-u} \right) \ln \delta_s + 12 \ln \left(\frac{m_h^2}{s} \right) \ln \delta_s - \frac{4}{3} \ln \left(\frac{m_h^2 \beta_h}{-t} \right) \ln \delta_s \\
&\quad - 3 \ln^2 \left(\frac{m_h^2}{s} \right) - 3 \ln^2 \left(\frac{m_h^2 \beta_h}{-u} \right) + \frac{1}{3} \ln^2 \left(\frac{m_h^2 \beta_h}{-t} \right) \\
&\quad + \left[\ln^2 \left(\frac{s}{m_h^2} \right) - \frac{\pi^2}{3} \right] \frac{A_{S2}}{2}, \tag{84}
\end{aligned}$$

and $\beta_H = 1 - m_h^2/s$.

The hard contribution to the real gluon emission process $qg \rightarrow qgh$ contains collinear singularities,

$$\sigma_{\text{real}} = \sigma_{\text{hard/collinear}} + \sigma_{\text{hard/non-collinear}}. \tag{85}$$

The hard/non-collinear terms arising from $i \rightarrow j$ parton splitting are finite and satisfy,

$$\begin{aligned}
E_g &> \delta_s \frac{\sqrt{s}}{2} \\
|S_{ij}| &> \delta_c s, \tag{86}
\end{aligned}$$

where δ_c is an arbitrary collinear cut-off and is typically $\ll \delta_s$. These terms can be integrated numerically using the amplitudes given in Appendix B.

2. Final State Collinear - qg channel

The hard collinear contribution to the partonic cross section from $q \rightarrow qg$ splitting in the final state is [75],

$$\begin{aligned}
\hat{\sigma}_{qg \rightarrow qgh}^{HC,f} &= \hat{\sigma}_{qg}^{LO} \frac{\alpha_s(\mu_R)}{2\pi} r_\Gamma \left(\frac{4\pi\mu_R^2}{s} \right)^\epsilon \left\{ \left(\frac{1}{\epsilon} - \ln \delta_c \right) C_F \left[2 \ln \left(\frac{\delta_s}{\beta_H} \right) + \frac{3}{2} \right] \right. \\
&\quad \left. - \frac{\pi^2}{3} - \ln^2 \left(\frac{\delta_s}{\beta_H} \right) + \frac{7}{2} \right\}. \tag{87}
\end{aligned}$$

3. Soft - gg channel

The contribution from soft gluon emission results from integrating the eikonal approximation to the $gg \rightarrow gh + g_{\text{soft}}$ matrix-element squared over the soft gluon phase space and yields,

$$|M_{gg \rightarrow gh}^{\text{soft}}|^2 = \frac{\alpha_s(\mu_R)}{\pi} r_\Gamma \left(\frac{4\pi\mu_R^2}{m_h^2} \right)^\epsilon \left\{ \frac{A_{g2}}{\epsilon^2} + \frac{A_{g1}}{\epsilon} + A_{g0} \right\} |M_{gg \rightarrow gh}^{(0)}|^2, \quad (88)$$

with

$$\begin{aligned} A_{g2} &= \frac{3}{2} N_c = \frac{9}{2}, \\ A_{g1} &= \frac{N_c}{2} \left\{ -6 \log(\delta_s) + \ln\left(\frac{m_h^2}{S_{12}}\right) + \ln\left(\frac{m_h^2 \beta_H}{-S_{13}}\right) + \ln\left(\frac{m_h^2 \beta_H}{-S_{23}}\right) \right\} \\ &\quad - \ln\left(\frac{S_{12}}{m_h^2}\right) A_{g2}, \\ A_{g0} &= \frac{N_c}{4} \left\{ 12 \ln^2(\delta_s) + \ln^2\left(\frac{m_h^2}{S_{12}}\right) + \ln^2\left(\frac{m_h^2 \beta_H}{-S_{13}}\right) + \ln^2\left(\frac{m_h^2 \beta_H}{-S_{23}}\right) \right. \\ &\quad \left. - 4 \ln \delta_s \left[\ln\left(\frac{m_h^2}{S_{12}}\right) + \ln\left(\frac{m_h^2 \beta_H}{-S_{13}}\right) + \ln\left(\frac{m_h^2 \beta_H}{-S_{23}}\right) \right] \right. \\ &\quad \left. + 2 \text{Li}_2\left(\frac{-S_{23}}{S_{12} \beta_H}\right) + 2 \text{Li}_2\left(\frac{-S_{13}}{S_{12} \beta_H}\right) \right\} \\ &\quad + \left[\ln^2\left(\frac{S_{12}}{m_h^2}\right) - \frac{\pi^2}{3} \right] \frac{A_{g2}}{2}. \end{aligned} \quad (89)$$

4. Final State Collinear - gg channel

The hard collinear contributions from gluon splitting in the final state are [75],

$$\begin{aligned} \hat{\sigma}_{gg \rightarrow ggh}^{HC,f} &= \hat{\sigma}_{gg \rightarrow ggh}^{LO} \frac{\alpha_s(\mu_R)}{2\pi} r_\Gamma \left(\frac{4\pi\mu_R^2}{s} \right)^\epsilon N_c \left\{ \left(\frac{1}{\epsilon} - \ln \delta_c \right) \left[2 \ln\left(\frac{\delta_s}{\beta_H}\right) + \frac{11}{6} \right] \right. \\ &\quad \left. - \frac{\pi^2}{3} - \ln^2\left(\frac{\delta_s}{\beta_H}\right) + \frac{67}{18} \right\}, \end{aligned} \quad (90)$$

$$\hat{\sigma}_{gg \rightarrow q\bar{q}h}^{HC,f} = \hat{\sigma}_{gg \rightarrow ggh}^{LO} \frac{\alpha_s(\mu_R)}{2\pi} r_\Gamma \left(\frac{4\pi\mu_R^2}{s} \right)^\epsilon n_{lf} \left\{ \left(\frac{1}{\epsilon} - \ln \delta_c \right) \left(-\frac{1}{3} \right) - \frac{5}{9} \right\}, \quad (91)$$

5. Initial State Collinear - all channels

The contribution from collinear splitting in the initial state is combined with the renormalization of the PDFs to obtain the result given in [75], applicable to all channels,

$$d\hat{\sigma}_{1+B \rightarrow 3+4+5}^{\text{initial+PDF}} = d\hat{\sigma}_{1+2' \rightarrow 3+4}^{\text{LO}} \frac{\alpha_s(\mu_R)}{2\pi} \frac{\Gamma(1-\epsilon)}{\Gamma(1-2\epsilon)} \left[\left(\frac{4\pi\mu_R^2}{s} \right)^\epsilon \tilde{f}_{2'/B}(z, \mu_F) + \frac{1}{\epsilon} \left(\frac{4\pi\mu_R^2}{\mu_F^2} \right)^\epsilon A_1^{sc}(2 \rightarrow 2' + 5) f_{2/B}(z, \mu_F) \right], \quad (92)$$

where the initial state hadron B splits into a parton $2'$ which scatters with the initial state parton 1 and a parton 5 which goes into the final state. The redefined parton distribution function \tilde{f} is given by [75]

$$\tilde{f}_{c/B}(x, \mu_f) = \sum_{c'} \int_x^{1-\delta_s \delta_{cc'}} \frac{dy}{y} f_{c'/B}(x/y, \mu_f) \tilde{P}_{cc'}(y), \quad (93)$$

$$\tilde{P}_{ij}(y) = P_{ij}(y) \ln \left(\delta_c \frac{1-y}{y} \frac{s}{\mu_f^2} \right) - P'_{ij}(y), \quad (94)$$

where P_{ij} and P'_{ij} are the $\mathcal{O}(\epsilon^0)$ and $\mathcal{O}(\epsilon)$ parts of the D -dimensional splitting function. The soft-collinear term A_1^{sc} , from the soft cutoff on initial state gluon emission, is given by [75]

$$A_1^{sc}(q \rightarrow qg) = C_F(2 \ln \delta_s + 3/2), \quad (95)$$

$$A_1^{sc}(g \rightarrow gg) = 2C_A \ln \delta_s + (11C_A - 2n_f)/6, \quad (96)$$

$$A_1^{sc}(g \rightarrow q\bar{q}) = 0. \quad (97)$$

E. Higher-dimensional gluon self interaction contribution

In Fig. 1 we give an example Feynman diagram which involves Higgs coupling in the $m_t \rightarrow \infty$ limit but contains an $\mathcal{O}(1/m_t^2)$ gluon-self coupling EFT vertex. Other diagrams of this type involve top quark loops as self-energy corrections of internal gluon propagators. These diagrams can be trivially calculated exactly, but we choose to use the EFT Lagrangian in Eq. (35) which gives the expansion to $\mathcal{O}(1/m_t^2)$. The contributions of these diagrams are of NLO order in α_s counting and $\mathcal{O}(1/m_t^2)$ in EFT power counting.

The contribution to the $0 \rightarrow q\bar{q}gh$ amplitude is

$$-8g_s^3 \frac{1}{m_t^2} \tilde{C}_4(\mathcal{T}_1 + \mathcal{T}_2) T^A = \frac{g_s^5}{30\pi^2 m_t^2} (T_1 + T_2) T^A, \quad (98)$$

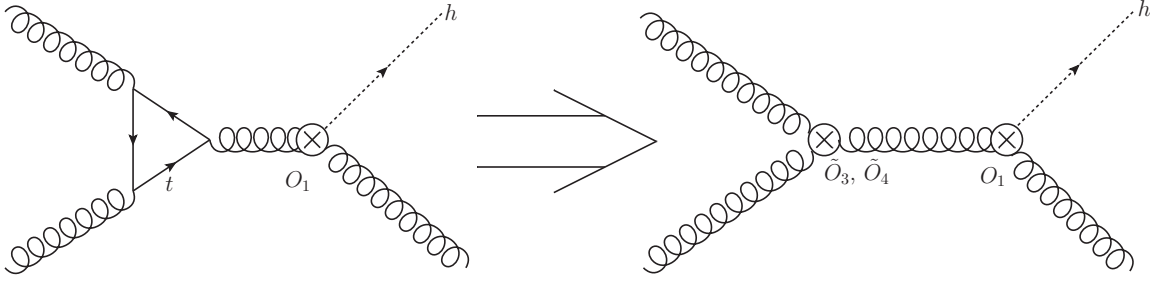


FIG. 1: An example diagram showing the $\mathcal{O}(1/m_t^2)$ gluon self-interaction vertex from integrating out the top quark. The Higgs is produced through the O_1 operator in the $m_t \rightarrow \infty$ limit, but the overall power of this Feynman diagram is still of $\mathcal{O}(1/m_t^2)$ and should be considered on the same footing as diagrams producing the Higgs through $1/m_t^2$ -suppressed dimension-7 operators.

while the contribution to the $0 \rightarrow gghh$ amplitude is

$$24g_s^2 f^{ABC} \tilde{C}_3 \left(\frac{S_{23}}{S_{12}} \mathcal{Y}_1^{\mu\nu\rho} + \frac{S_{12}}{S_{31}} \mathcal{Y}_2^{\mu\nu\rho} + \frac{S_{31}}{S_{23}} \mathcal{Y}_3^{\mu\nu\rho} \right) \quad (99)$$

$$= \frac{1}{120\pi^2} g_s^5 f^{ABC} \left(\frac{S_{23}}{S_{12}} \mathcal{Y}_1^{\mu\nu\rho} + \frac{S_{12}}{S_{31}} \mathcal{Y}_2^{\mu\nu\rho} + \frac{S_{31}}{S_{23}} \mathcal{Y}_3^{\mu\nu\rho} \right), \quad (100)$$

where the T_i and Y_i tensor structures are given in Eqs. (37),(38),(42)-(44).

VI. NLO REAL EMISSION HELICITY AMPLITUDES

The helicity amplitudes for the production of Higgs plus two jets in the $m_t \rightarrow \infty$ limit, i.e. the O_1 contribution, was worked out long ago [77, 78]. We will calculate the amplitudes for dimension-7 operators. The all-gluon amplitudes will be given in this section, while amplitudes involving quarks will be given in Appendix B. The O_4 and O_5 operators, which involve quark bilinears, do not contribute to tree amplitudes without external quark legs, so only O_1 and O_3 will appear here.

Amplitudes for the G^3 operator without the Higgs, as a model for higher-dimensional modifications of the SM QCD sector, were studied in Refs. [79, 80]. These references found that the G^3 and G^2 amplitudes do not interfere with each other unless there are at least 3 jets in the final states. Our amplitudes for O_3 must reproduce these amplitudes in the limit of zero Higgs momentum, resulting in vanishing O_1 - O_3 interference. The above references also proposed MHV formulas for n -gluon G^3 amplitudes involving 3 minus-helicities and

$n - 3$ plus helicities. We will verify that these MHV formulas hold for the O_3 $gggh$ and $ggggh$ amplitudes, i.e. G^3 amplitudes at non-zero (and non-lightlike) momentum insertion. This is expected, as Ref. [79, 80] already found MHV formulas for the G^2 operator to be valid at finite momentum, for Higgs production in the $m_t \rightarrow \infty$ limit.

For convenience, we will first give the lowest-order $gggh$ amplitude for Higgs plus jet production again, in helicity amplitude notation rather than tensor structure notation. The O_1 contributions, proportional to C_1 , are

$$im^{O_1}(1^+, 2^+, 3^+, h) = \frac{2g_s m_h^4}{\langle 12 \rangle \langle 23 \rangle \langle 31 \rangle}, \quad (101)$$

$$im^{O_1}(1^-, 2^+, 3^+, h) = -\frac{2g_s [23]^4}{[12][23][31]}. \quad (102)$$

The O_3 contributions, proportional to C_3 , are

$$im^{O_3}(1^+, 2^+, 3^+, h) = \frac{-3[12][23][31]}{\Lambda^2}, \quad (103)$$

$$im^{O_3}(1^-, 2^+, 3^+, h) = 0, \quad (104)$$

in agreement with Ref. [81]. As p_T becomes large, in the Higgs rest frame, the initial and final state jets become much more energetic than the Higgs, so the $m_h \rightarrow 0$ limit of the above amplitudes, Eqs. (101)-(104), is particularly interesting. In this limit, the $-++$ amplitude is non-zero for O_1 , but vanishes for O_3 , so there is no interference between O_1 and O_3 for this helicity configuration. Meanwhile, the $+++$ amplitude is non-zero as $m_h \rightarrow 0$ for O_3 , but vanishes as a quartic power in the $m_h \rightarrow 0$ limit for O_1 , as seen in Eq. (101). Therefore, we expect the $gggh$ amplitude to not receive large enhancements from the dimension-7 O_3 operator at large p_T , which means the $m_t \rightarrow \infty$ approximation should work well for Higgs differential distribution even at moderately large p_T .

Now we will give the $ggggh$ tree amplitudes for O_3 . They are:

$$im^{O_3}(1^+, 2^+, 3^+, 4^+, h) = \frac{g_s}{\langle 12 \rangle \langle 23 \rangle \langle 34 \rangle \langle 41 \rangle} \left(3i S_{12} S_{23} S_{34} - \frac{3}{2} i S_{12} [31] \langle 1p_H 2 \rangle \langle 23 \rangle - \frac{3}{2} i S_{12} [42] \langle 2p_H 1 \rangle \langle 14 \rangle \right) + 3 \text{ cyclic permutations of } (1 \rightarrow 2 \rightarrow 3 \rightarrow 4 \rightarrow 1), \quad (105)$$

$$im^{O_3}(1^-, 2^-, 3^-, 4^+, h) = \frac{3i g_s \langle 12 \rangle^2 \langle 23 \rangle^2 \langle 34 \rangle^2}{\langle 12 \rangle \langle 23 \rangle \langle 34 \rangle \langle 41 \rangle}, \quad (106)$$

$$im^{O_3}(1^-, 2^-, 3^+, 4^+, h) = 0. \quad (107)$$

We comment on the massless Higgs limit again. For the $--++$ helicity configuration, the O_3 contribution vanishes, while for the $++++$ helicity configuration, the O_1 contribution [77, 78] vanishes like a quartic power in the massless Higgs limit. However, for the $---+$ helicity configuration, neither the O_3 nor O_1 contribution vanishes in the limit $m_h \rightarrow 0$ (though the latter vanishes in the limit $p_h \rightarrow 0$), so the O_1 - O_3 non-interference at high p_T is no longer true at NLO.

The amplitudes in Eqs. (103) and (106) are unchanged from the MHV formulas for G^3 at zero momentum in Ref. [79, 80]. Furthermore, Refs. [80, 82] explored the use of CSW rules [83] to build non-MHV amplitudes from MHV sub-amplitudes for the G^3 operator. We confirm that the $++++$ amplitude in Eq. (105) agrees with the CSW construction with G^3 inserted at non-zero momentum. The vanishing of the $--++$ amplitude in Eq. (107) is explained by the fact that this helicity configuration cannot be built from MHV sub-amplitudes [80, 82].

We have checked that the squared matrix elements from the helicity amplitudes, presented in this section and Appendix B, agree with the automated tree-level calculation by MadGraph5_aMC@NLO [84], using a UFO model file [85] for the dimension-7 operators which we created using FeynRules [69].

VII. PHENOMENOLOGY

In this section, we present LO, $\mathcal{O}(\alpha_s^3)$, and NLO, $\mathcal{O}(\alpha_s^4)$, results for the Higgs transverse momentum distributions resulting from the effective operators, using the basis of Eq. 26. All curves use NLO CJ12 PDFs [86] with $\mu_F = \mu_R = m_h = 126$ GeV, $m_t = 173$ GeV, and the 2-loop evolution of α_s , with $\alpha_s(126 \text{ GeV}) = 0.112497$. The O_1 contribution, with C_1 defined in Eq. (31) to include $\mathcal{O}(m_h^2/m_t^2)$ corrections, is equivalent to the $m_t \rightarrow \infty$ result rescaled by an overall correction factor. The sum of all contributions, from O_1 , O_3 , O_5 , and the gluon self-interaction operators in Section V E, gives the full result up to $\mathcal{O}(m_h^4/m_t^4)$ corrections in the SM limit. We use the SM values for the C_i in our plots, but the individual results can be trivially rescaled for BSM coefficients.

A. LO results

At LO, O_3 does not contribute to quark channels and O_5 does not contribute to the gg channel. In Fig. 2, we plot the LO p_T distribution resulting from the individual operators, and in Fig. 3, the same plot is broken up into different partonic channels. The curves labeled as O_i - O_j are proportional to $C_i C_j$, where in this section we use the $\mathcal{O}(\alpha_s)$ results for the SM $C_i^{\text{SM,pole}}$. We can see that the O_1 - O_1 result declines as p_T increases due to the decrease of the gg parton luminosity function, while the O_1 - O_5 interference term (which is negative) grows in relative significance at large p_T due to the effects of terms of $\mathcal{O}(p_T^2/m_t^2)$ in the quark-gluon channel. The O_1 - O_3 interference term declines even more rapidly than the O_1 result at high p_T , due to the non-interference of the tree-level amplitudes from O_1 and O_3 in the soft Higgs limit. As seen in the real emission section, at tree-level the two operators cannot interfere in the soft Higgs limit unless there are 3 or more jets in the final state. Also shown is the exact LO result of Ref. [37], including the effects of the top loop exactly. As made clear also in Ref. [24], the exact and the EFT results diverge for $p_T > 150$ GeV.⁵

Since for LO diagrams without external external quark lines, O_3 is the only needed operator that is not from a rescaling of the $m_t \rightarrow \infty$ limit, we have an explanation for the excellent agreement between the O_1 result and the exact result in the gg channel shown

⁵ After accounting for differing input parameters and basis for the dimension-7 operators, our results are in agreement with Ref. [87].

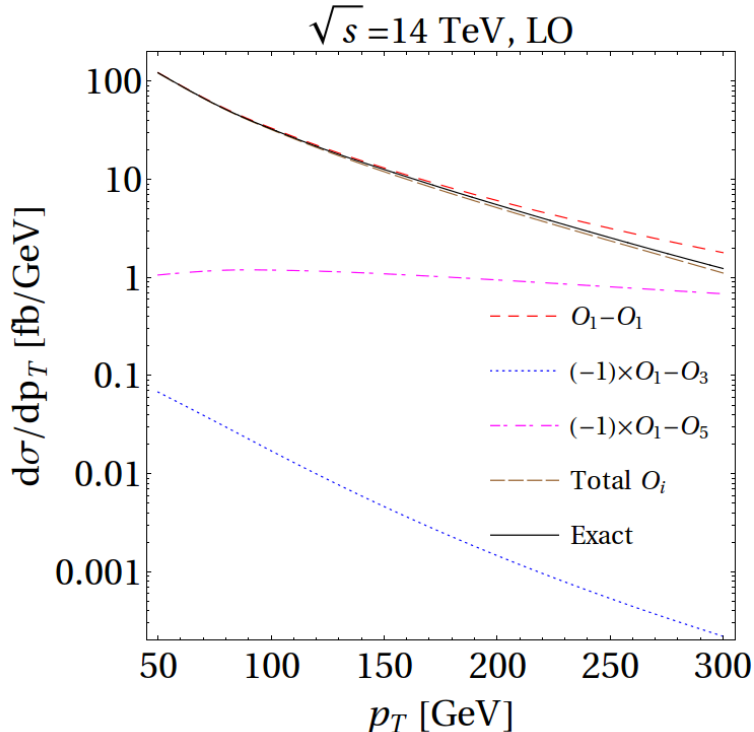


FIG. 2: Leading order Higgs transverse momentum distributions from the dimension-5 and dimension-7 EFT operators for Higgs plus jet production at LO using CJ12 NLO PDFs with $\mu_R = \mu_F = m_h$. The curves use the $\mathcal{O}(\alpha_s)$ SM values of the C_i and include terms to $\mathcal{O}(1/m_t^2)$.

in Fig. 2, even at rather large p_T . For the qg -channel, on the other hand, the growing importance of O_5 explains the much worse agreement between the EFT result and the exact result at large p_T . At small p_T , though, the tree-level $qg \rightarrow qh$ amplitude factorizes into the collinear splitting $q \rightarrow qg$ and the on-shell $gg \rightarrow h$ amplitude, which explains the good agreement between the O_1 result and the exact result in the qg -channel. For the qq channel which neither enjoys the special properties of the O_3 helicity amplitudes nor factorizes into gluon sub-amplitudes, we see that the $m_t \rightarrow \infty$ approximation with scaling breaks down even at low $p_T \sim 50$ GeV. In Figs. 4 and 5 we plot the deviation of the O_1 result and the total result from the exact result. We again see the remarkably tame deviation in the gg channel from the exact result, while observing that including all dimension-7 operators gives a better approximation to the exact p_T distribution than including the effects of O_1 alone, especially for $p_T < m_h$.

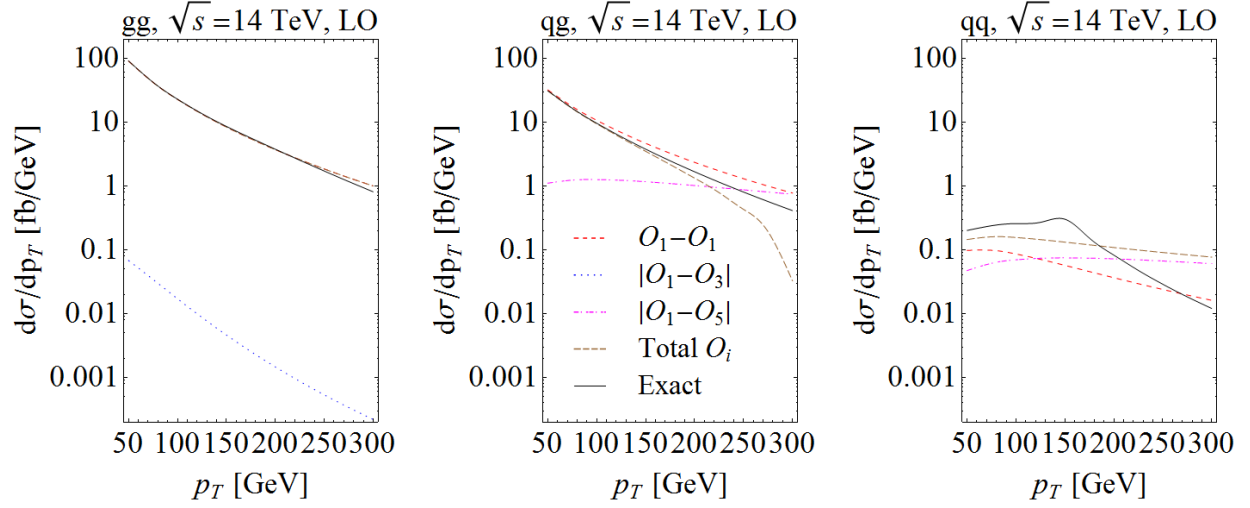


FIG. 3: Leading order Higgs transverse momentum distributions from the dimension-5 and dimension-7 EFT operators for Higgs plus jet production at LO using CJ12 NLO PDFs with $\mu_R = \mu_F = m_h$. The curves use the $\mathcal{O}(\alpha_s)$ SM values of the C_i and include terms to $\mathcal{O}(1/m_t^2)$. Contributions from gg , qg , and qq partonic channels are shown separately.

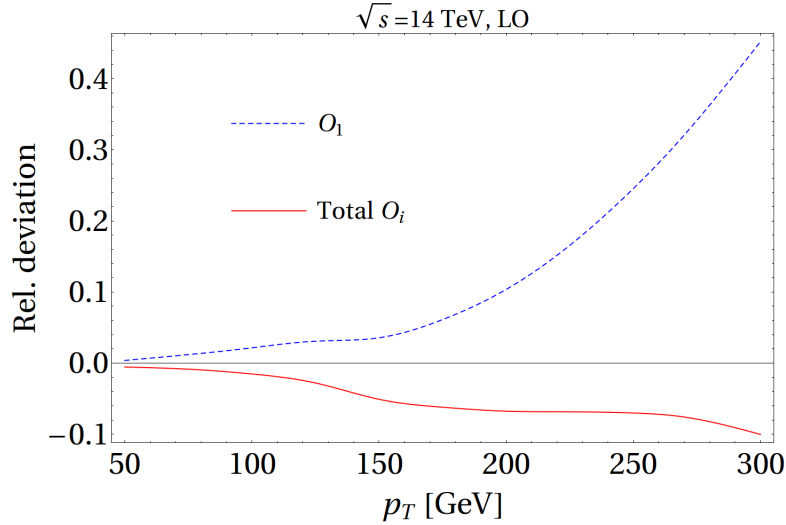


FIG. 4: Deviations of the EFT predictions including all dimension-5 and dimension-7 operators (solid curve) from the exact result for Higgs plus jet production at LO using CJ12 NLO PDFs with $\mu_R = \mu_F = m_h$. The curves use the $\mathcal{O}(\alpha_s)$ SM values of the C_i and include terms to $\mathcal{O}(1/m_t^2)$. The dotted curve includes only the contribution from O_1 .

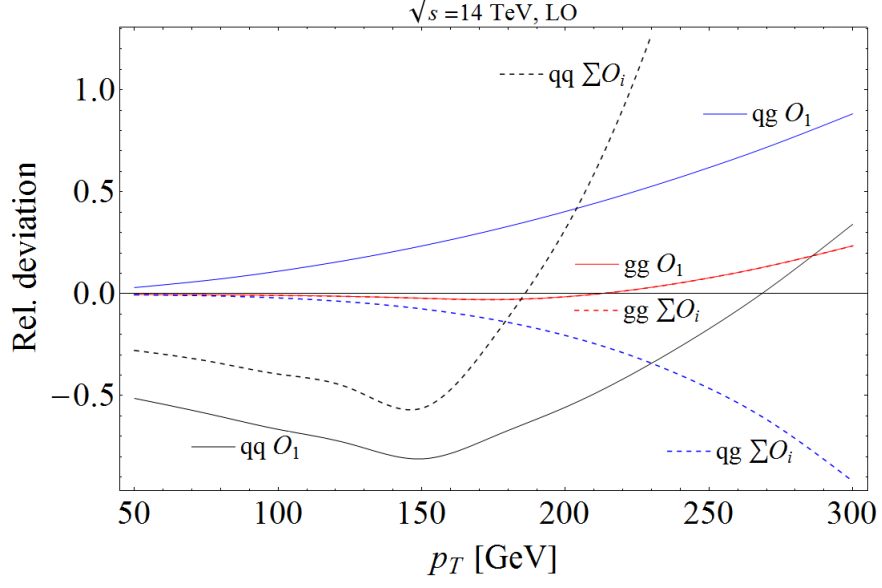


FIG. 5: Deviations of the EFT predictions from the exact results (dotted curves) , broken up into partonic channels, for Higgs plus jet production at LO using CJ12 NLO PDFs with $\mu_R = \mu_F = m_h$. The curves use the $\mathcal{O}(\alpha_s)$ SM values of the C_i and include terms to $\mathcal{O}(1/m_t^2)$. The solid curves includes only the contribution from O_1 . The red dashed and red solid curves are indistinguishable.

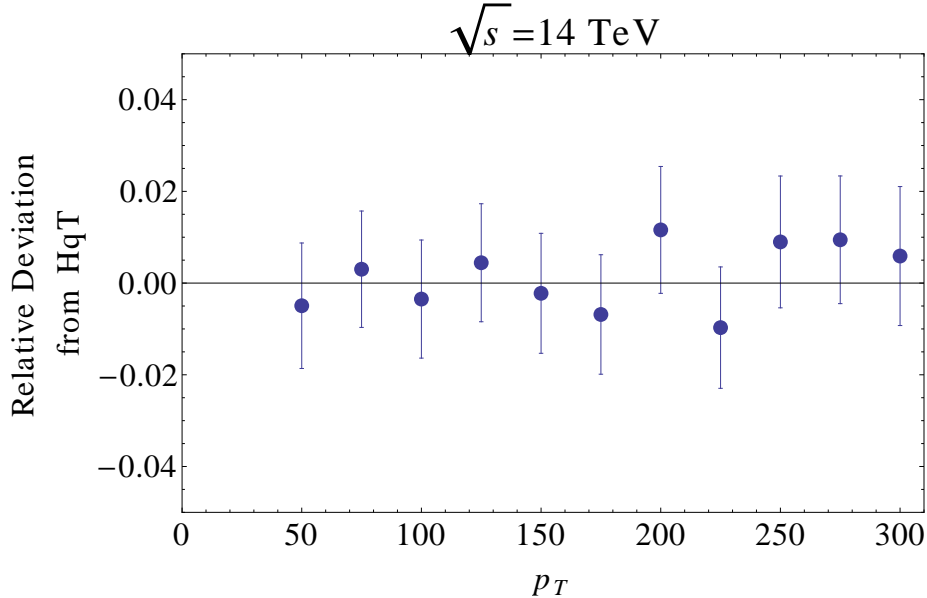


FIG. 6: Deviation of our NLO result for the Higgs p_T distribution in the large m_t limit from the results of the HqT 2.0 program [87] using $\delta_s = 10^{-3}$, and $\delta_c = \delta_s/200$ for $p_T \geq 75$ GeV and $\delta_c = \delta_s/400$ for $p_T = 50$ GeV.

B. Numerical accuracy at NLO

Our NLO results are derived using phase space slicing with 2 cut-offs, δ_c and δ_s . To show the accuracy of our implementation of phase space slicing, in Fig. 6, we show the deviation of our NLO result for the $m_t \rightarrow \infty$ limit from the result produced by HqT 2.0 [87]. (The errors are statistical). We find agreement at the percent level. The variation of $d\sigma/dp_T$ with δ_s for the O_3 and O_5 operators individually (using the SM $\mathcal{O}(\alpha_s^2)$ values for the $C_i^{\text{SM,pole}}$ coefficients) is plotted in Fig. 7 for fixed $\delta_c = 5 \times 10^{-6}$ and for $p_T = 100$ GeV. We see that at the percent level, our results are independent of the choice of soft cutoff. Similarly, we have verified there is no dependence on the collinear cutoff when $\delta_c \ll \delta_s$. Our results in the following sections use $\delta_c = 5 \times 10^{-6}$ (except for the O_1 result at $p_T = 50.0$ GeV, for which we use one half this value) and $\delta_s = 10^{-3}$. All the plots are made by computing at $\delta p_T = 25$ GeV intervals, joined together by smooth curves, and it should be kept in mind that an error of $\sim 1 - 2\%$ is present.

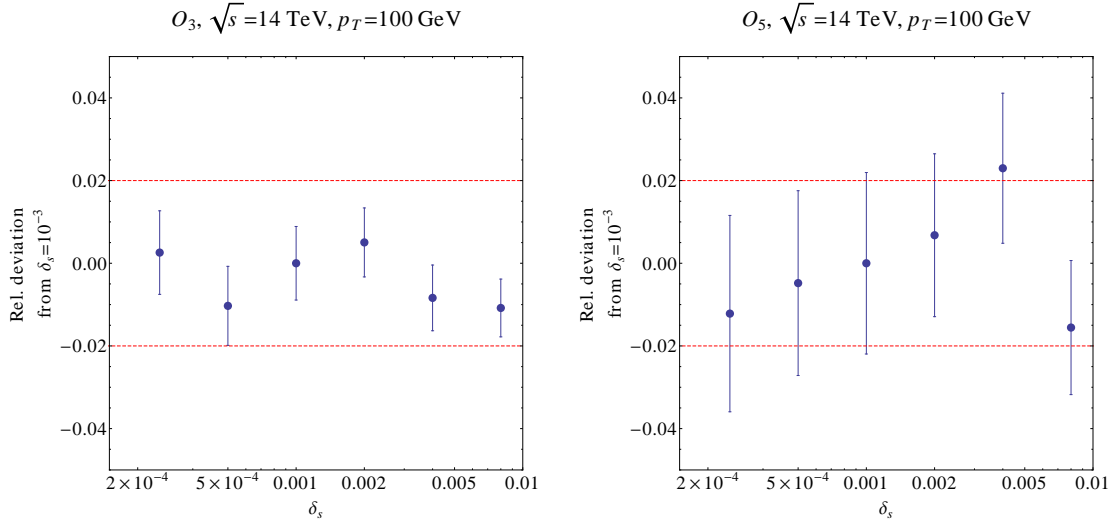


FIG. 7: Dependence of the NLO result for the Higgs p_T distribution on the soft cutoff, δ_s , including only the interference of O_1 with O_3 (LHS) and O_1 with O_5 (RHS). The collinear cutoff is taken to be $\delta_c = 5 \times 10^{-6}$. The result with $\delta_s = 10^{-3}$ is normalized to 1.

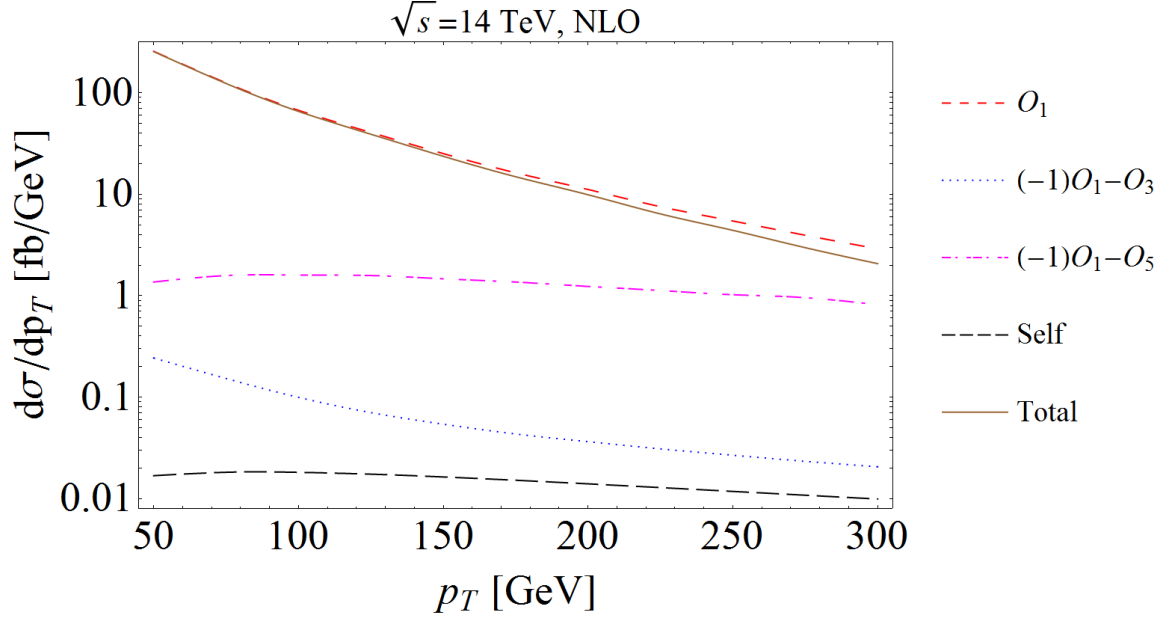


FIG. 8: Next-to-leading order Higgs transverse momentum distributions from the EFT dimension-5 and dimension-7 operators, using the SM values of $C_i^{\text{SM,pole}}$ to $\mathcal{O}(\alpha_s^2)$ and include terms only to $\mathcal{O}(1/m_t^2)$.

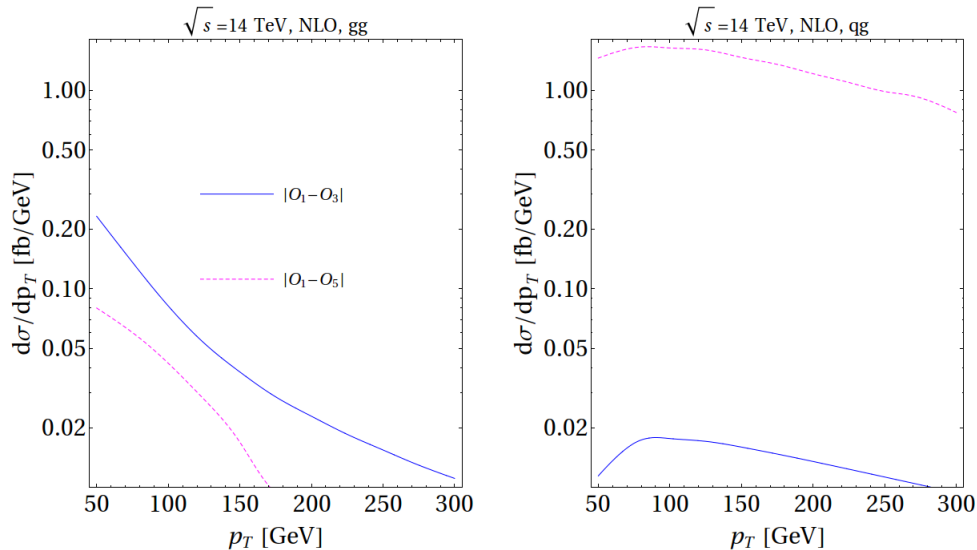


FIG. 9: Comparison of the sizes of O_3 and O_5 contributions in the gg and qg channels at NLO.

C. NLO results

In Fig. 8, we plot the contributions of the dimension-5 and dimension-7 EFT operators to the NLO p_T distributions. The NLO plots use the $\mathcal{O}(\alpha_s^2)$ expressions for the $C_i^{\text{SM,pole}}$ and include terms only to $\mathcal{O}(1/m_t^2)$. Compared with the LO plot in Fig. 2, an important change is that the dimension-7 O_3 contribution no longer shows the property of declining faster than the dimension-5 O_1 contribution (because interference between O_3 and O_1 amplitudes in the soft Higgs limit starts at NLO), although O_5 is still dominant at large p_T . The curve labeled “self” is the small contribution from the $\mathcal{O}(1/m_t^2)$ gluon self-couplings of Eq. 35. The dimension-7 contributions to the gg and qg individual channels are shown in Fig. 9. In the gg channel, the O_5 operator starts to have non-vanishing contribution at NLO, but the contribution remains small compared with O_3 , partly because O_5 only affects diagrams involving external quark legs or internal quark loops. In the qg channel, the O_3 operator starts to have non-vanishing contribution at NLO, but the contribution remains small compared with O_5 . Therefore, we should still associate O_3 primarily with the gg channel, and O_5 primarily with channels involving initial-state quarks.

In order to quantify the size of our results, we define a p_T dependent K-factor:

$$K(p_T) = \frac{\frac{d\sigma}{dp_T}(\text{NLO})}{\frac{d\sigma}{dp_T}(\text{LO})}, \quad (108)$$

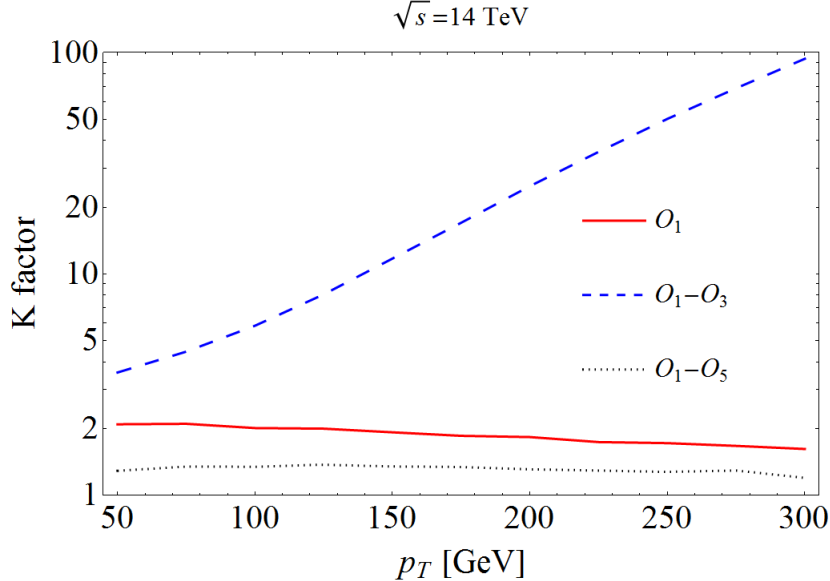


FIG. 10: The NLO p_T -dependent K-factor for each of the operators, as defined in Eq. 108.

where in our plots both the NLO and LO curves use CJ12 PDFs with the 2-loop evolution of α_s . We plot the K factor separately for the contributions from O_1 and for the contributions from the interference of O_1 with O_3 and O_5 . The results use the SM values of $C_i^{\text{SM,pole}}$, but can be rescaled appropriately for BSM models. In Fig. 10, we see that the NLO K-factors for O_1 and O_5 are always of order unity, while the O_3 K-factor reaches huge values at large p_T , reflecting the fact that the vanishing interference between the O_1 and O_3 helicity amplitudes in the soft Higgs limit no longer holds at one-loop level.

In Fig. 11, we show the NLO p_T dependent K-factors for each partonic channel. We can see that in going from the contribution of only O_1 to the sum of the contributions from all operators, the K-factor hardly changes in the gg -channel, while there are significant changes in the qg and qq channels. This is not surprising given the high p_T suppression of the O_3 contribution and the lack of an O_5 contribution in the all-gluon channel at LO, while the NLO effects are not large enough to destroy the agreement with the contribution of O_1 alone. In Fig. 12 we observe that when all partonic channels are summed up, the K-factor only shows modest changes [41, 42] due to the dominance of the gg channel.

Our K-factors plots are for SM Higgs production, with the non-logarithmic terms $\hat{C}_3^{(1)}$ and $\hat{C}_5^{(1)}$ in Eq. (11), (13) set to zero. It is straightforward to scale the K factors to reflect the effects of BSM physics. Define the K-factors corresponding to O_i as K^i , and define the

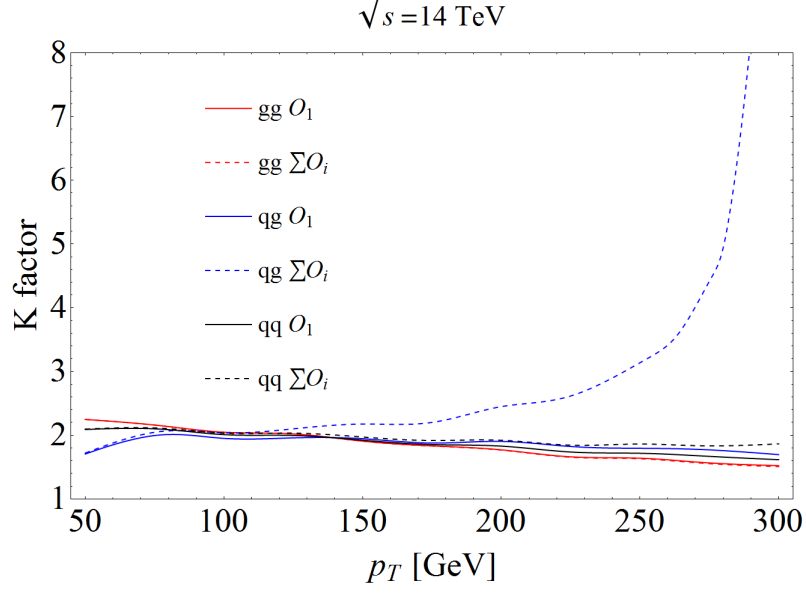


FIG. 11: The NLO p_T -dependent K-factor, broken up into partonic channels.

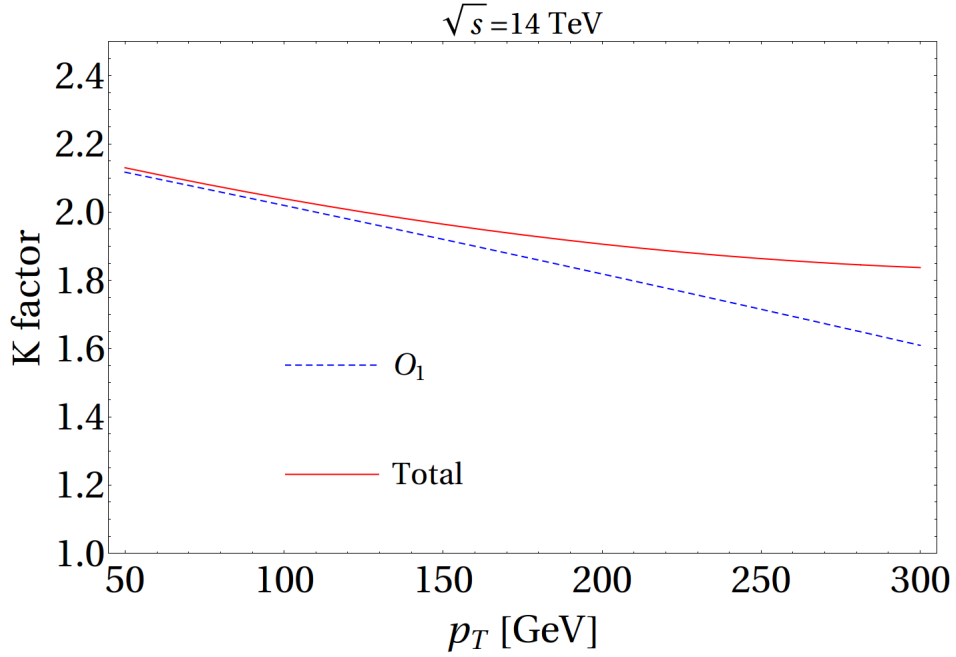


FIG. 12: The NLO p_T -dependent K-factor, broken up into partonic channels, summed over all partonic channels.

expansion in α_s for SM and BSM coefficients,

$$\begin{aligned}
 C_i^{\text{SM}} &= \alpha_s C_i^{(0,\text{SM})} + \alpha_s^2 C_i^{(1,\text{SM})}, \\
 C_i^{\text{BSM}} &= \alpha_s C_i^{(0,\text{BSM})} + \alpha_s^2 C_i^{(1,\text{BSM})}.
 \end{aligned}
 \tag{109}$$

The K-factor for a BSM model can be derived to $O(\alpha_s)$ by the rescaling,

$$\begin{aligned}
\frac{K^{1,\text{BSM}}}{K^{1,\text{SM}}} &= 1 + 2\alpha_s \left(\frac{C_1^{(1,\text{BSM})}}{C_1^{(0,\text{BSM})}} - \frac{C_1^{(1,\text{SM})}}{C_1^{(0,\text{SM})}} \right), \\
\frac{K^{1,\text{BSM}}}{K^{1,\text{SM}}} &= 1 + \alpha_s \left(\frac{C_1^{(1,\text{BSM})}}{C_1^{(0,\text{BSM})}} - \frac{C_1^{(1,\text{SM})}}{C_1^{(0,\text{SM})}} + \frac{C_5^{(1,\text{BSM})}}{C_5^{(0,\text{BSM})}} - \frac{C_5^{(1,\text{SM})}}{C_5^{(0,\text{SM})}} \right), \\
\frac{K^{1,\text{BSM}}}{K^{1,\text{SM}}} &= 1 + \alpha_s \left(\frac{C_1^{(1,\text{BSM})}}{C_1^{(0,\text{BSM})}} - \frac{C_1^{(1,\text{SM})}}{C_1^{(0,\text{SM})}} + \frac{C_3^{(1,\text{BSM})}}{C_3^{(0,\text{BSM})}} - \frac{C_3^{(1,\text{SM})}}{C_3^{(0,\text{SM})}} \right). \tag{110}
\end{aligned}$$

VIII. CONCLUSION

We used an effective field theory containing strong gluon-Higgs-quark operators to dimension-7 to parameterize either non-SM couplings or the effect of a finite top mass within the SM. We calculated the NLO, $\mathcal{O}(\alpha_s^4)$, contribution to the p_T spectrum for Higgs plus jet production, including effects of $\mathcal{O}(1/\Lambda^2)$, for arbitrary values of the coefficients, C_i , of the effective Lagrangian. There are 3 dimension-7 operators which contribute to Higgs plus jet production: $O_6 \cong m_h^2 O_1$, O_3 , and O_5 . The operator O_6 rescales the overall gluon fusion rate for Higgs production and is constrained to be close to the SM value. The contribution from O_3 , mainly in the gg channel, is suppressed at LO for large p_T since it vanishes in the soft Higgs limit, and remains numerically small at NLO, making it difficult to observe new physics in this channel, and also suppressing the dependence on the top quark mass. The contribution from O_5 , which is mainly in the qg channel, is significant at large p_T . Hence, BSM physics will be most readily accessible if it contains a significant enhancement of C_5 over the SM value. We studied the renormalization of the dimension-7 operators, which makes it possible to regulate the UV divergence of the one-loop amplitudes and to use renormalization group running, from the BSM scale down to the Higgs mass scale, to resum large logarithms.

When the operator coefficients are set to their SM values, we obtain the $\mathcal{O}(1/m_t^2)$ corrections to the NLO rate for Higgs plus jet production, modulo the non-logarithmic terms in the NLO matching coefficients in Eqs. (11),(13) to be presented shortly in a forthcoming work. These corrections are well behaved in the gg channel, but become increasingly large in the qg channel as p_T is increased above m_h . This observation is in agreement with Ref. [41]. We present p_T dependent K factors which can be easily rescaled to include BSM physics.

Acknowledgments

The work of SD and IL is supported the U.S. Department of Energy under grant No. DE-AC02-98CH10886. The work of MZ is supported by NSF grant PHY-1316617. We thank Lance Dixon, Duff Neill, and George Sterman for useful discussions.

-
- [1] Updated coupling measurements of the Higgs boson with the ATLAS detector using up to 25 fb^{-1} of proton-proton collision data. Technical Report ATLAS-CONF-2014-009, CERN, Geneva, Mar 2014.
- [2] Precise determination of the mass of the Higgs boson and studies of the compatibility of its couplings with the standard model. Technical Report CMS-PAS-HIG-14-009, CERN, Geneva, 2014.
- [3] S. Dittmaier et al. Handbook of LHC Higgs Cross Sections: 1. Inclusive Observables. 2011.
- [4] S. Dittmaier, S. Dittmaier, C. Mariotti, G. Passarino, R. Tanaka, et al. Handbook of LHC Higgs Cross Sections: 2. Differential Distributions. 2012.
- [5] Bernd A. Kniehl and Michael Spira. Low-energy theorems in Higgs physics. *Z.Phys.*, C69:77–88, 1995.
- [6] M. Spira, A. Djouadi, D. Graudenz, and P.M. Zerwas. Higgs boson production at the LHC. *Nucl.Phys.*, B453:17–82, 1995.
- [7] S. Dawson. Radiative corrections to Higgs boson production. *Nucl.Phys.*, B359:283–300, 1991.
- [8] N. Arkani-Hamed, A.G. Cohen, E. Katz, and A.E. Nelson. The Littlest Higgs. *JHEP*, 0207:034, 2002.
- [9] Roberto Contino, Yasunori Nomura, and Alex Pomarol. Higgs as a holographic pseudoGoldstone boson. *Nucl.Phys.*, B671:148–174, 2003.
- [10] Ian Low and Alessandro Vichi. On the production of a composite Higgs boson. *Phys.Rev.*, D84:045019, 2011.
- [11] M. Carena, S. Heinemeyer, O. Stl, C.E.M. Wagner, and G. Weiglein. MSSM Higgs Boson Searches at the LHC: Benchmark Scenarios after the Discovery of a Higgs-like Particle. *Eur.Phys.J.*, C73:2552, 2013.
- [12] Marcela Carena, Stefania Gori, Nausheen R. Shah, Carlos E.M. Wagner, and Lian-Tao Wang. Light Stops, Light Staus and the 125 GeV Higgs. *JHEP*, 1308:087, 2013.
- [13] Christophe Grojean, Ennio Salvioni, Matthias Schlaffer, and Andreas Weiler. Very boosted Higgs in gluon fusion. *JHEP*, 1405:022, 2014.
- [14] Aleksandr Azatov and Ayan Paul. Probing Higgs couplings with high p_T Higgs production. *JHEP*, 1401:014, 2014.

- [15] Ian Low, Riccardo Rattazzi, and Alessandro Vichi. Theoretical Constraints on the Higgs Effective Couplings. *JHEP*, 1004:126, 2010.
- [16] Malte Buschmann, Christoph Englert, Dorival Goncalves, Tilman Plehn, and Michael Spannowsky. Resolving the Higgs-Gluon Coupling with Jets. *Phys.Rev.*, D90:013010, 2014.
- [17] Matthias Schlaffer, Michael Spannowsky, Michihisa Takeuchi, Andreas Weiler, and Chris Wymant. Boosted Higgs Shapes. 2014.
- [18] Aleksandr Azatov and Jamison Galloway. Light Custodians and Higgs Physics in Composite Models. *Phys.Rev.*, D85:055013, 2012.
- [19] S. Dawson and E. Furlan. A Higgs Conundrum with Vector Fermions. *Phys.Rev.*, D86:015021, 2012.
- [20] M. Gillioz, R. Grober, C. Grojean, M. Muhlleitner, and E. Salvioni. Higgs Low-Energy Theorem (and its corrections) in Composite Models. *JHEP*, 1210:004, 2012.
- [21] Sally Dawson, Elisabetta Furlan, and Ian Lewis. Unravelling an extended quark sector through multiple Higgs production? *Phys.Rev.*, D87:014007, 2013.
- [22] Andrea Banfi, Adam Martin, and Veronica Sanz. Probing top-partners in Higgs + jets. 2013.
- [23] Duff Neill. Two-Loop Matching onto Dimension Eight Operators in the Higgs-Gluon Sector. 2009.
- [24] Robert V. Harlander and Tobias Neumann. Probing the nature of the Higgs-gluon coupling. *Phys.Rev.*, D88:074015, 2013.
- [25] Robert V. Harlander and William B. Kilgore. Next-to-next-to-leading order Higgs production at hadron colliders. *Phys.Rev.Lett.*, 88:201801, 2002.
- [26] V. Ravindran, J. Smith, and W. L. van Neerven. NNLO corrections to the total cross-section for Higgs boson production in hadron hadron collisions. *Nucl.Phys.*, B665:325–366, 2003.
- [27] Charalampos Anastasiou and Kirill Melnikov. Higgs boson production at hadron colliders in NNLO QCD. *Nucl.Phys.*, B646:220–256, 2002.
- [28] Charalampos Anastasiou, Kirill Melnikov, and Frank Petriello. Fully differential Higgs boson production and the di-photon signal through next-to-next-to-leading order. *Nucl.Phys.*, B724:197–246, 2005.
- [29] Stefano Catani and Massimiliano Grazzini. An NNLO subtraction formalism in hadron collisions and its application to Higgs boson production at the LHC. *Phys.Rev.Lett.*, 98:222002, 2007.

- [30] V. Ravindran, J. Smith, and W.L. Van Neerven. Next-to-leading order QCD corrections to differential distributions of Higgs boson production in hadron hadron collisions. *Nucl.Phys.*, B634:247–290, 2002.
- [31] Robert V. Harlander and Kemal J. Ozeren. Finite top mass effects for hadronic Higgs production at next-to-next-to-leading order. *JHEP*, 0911:088, 2009.
- [32] Alexey Pak, Mikhail Rogal, and Matthias Steinhauser. Finite top quark mass effects in NNLO Higgs boson production at LHC. *JHEP*, 1002:025, 2010.
- [33] K.G. Chetyrkin, Bernd A. Kniehl, and M. Steinhauser. Decoupling relations to $O(\alpha_s^3)$ and their connection to low-energy theorems. *Nucl.Phys.*, B510:61–87, 1998.
- [34] Y. Schroder and M. Steinhauser. Four-loop decoupling relations for the strong coupling. *JHEP*, 0601:051, 2006.
- [35] K.G. Chetyrkin, Johann H. Kuhn, and Christian Sturm. QCD decoupling at four loops. *Nucl.Phys.*, B744:121–135, 2006.
- [36] Michael Kramer, Eric Laenen, and Michael Spira. Soft gluon radiation in Higgs boson production at the LHC. *Nucl.Phys.*, B511:523–549, 1998.
- [37] R. Keith Ellis, I. Hinchliffe, M. Soldate, and J.J. van der Bij. Higgs Decay to $\tau^+ \tau^-$: A Possible Signature of Intermediate Mass Higgs Bosons at the SSC. *Nucl.Phys.*, B297:221, 1988.
- [38] U. Baur and E.W. Nigel Glover. Higgs Boson Production at Large Transverse Momentum in Hadronic Collisions. *Nucl.Phys.*, B339:38–66, 1990.
- [39] D. de Florian, M. Grazzini, and Z. Kunszt. Higgs production with large transverse momentum in hadronic collisions at next-to-leading order. *Phys.Rev.Lett.*, 82:5209–5212, 1999.
- [40] Christopher J. Glosser and Carl R. Schmidt. Next-to-leading corrections to the Higgs boson transverse momentum spectrum in gluon fusion. *JHEP*, 0212:016, 2002.
- [41] Robert V. Harlander, Tobias Neumann, Kemal J. Ozeren, and Marius Wiesemann. Top-mass effects in differential Higgs production through gluon fusion at order α_s^4 . *JHEP*, 1208:139, 2012.
- [42] Massimiliano Grazzini and Hayk Sargsyan. Heavy-quark mass effects in Higgs boson production at the LHC. *JHEP*, 1309:129, 2013.
- [43] E. Bagnaschi, G. Degrossi, P. Slavich, and A. Vicini. Higgs production via gluon fusion in the POWHEG approach in the SM and in the MSSM. *JHEP*, 1202:088, 2012.

- [44] Tobias Neumann and Marius Wiesemann. Finite top-mass effects in gluon-induced Higgs production with a jet-veto at NNLO. 2014.
- [45] Wai-Yee Keung and Frank J. Petriello. Electroweak and finite quark-mass effects on the Higgs boson transverse momentum distribution. *Phys.Rev.*, D80:013007, 2009.
- [46] Radja Boughezal, Fabrizio Caola, Kirill Melnikov, Frank Petriello, and Markus Schulze. Higgs boson production in association with a jet at next-to-next-to-leading order in perturbative QCD. *JHEP*, 1306:072, 2013.
- [47] Thomas Becher, Guido Bell, Christian Lorentzen, and Stefanie Marti. The transverse-momentum spectrum of Higgs bosons near threshold at NNLO. 2014.
- [48] Thomas Becher, Guido Bell, Christian Lorentzen, and Stefanie Marti. Transverse-momentum spectra of electroweak bosons near threshold at NNLO. *JHEP*, 1402:004, 2014.
- [49] Fa Peng Huang, Chong Sheng Li, Hai Tao Li, and Jian Wang. Renormalization-group improved predictions for Higgs boson production at large p_T . 2014.
- [50] V. Del Duca, W. Kilgore, C. Oleari, C. Schmidt, and D. Zeppenfeld. Higgs + 2 jets via gluon fusion. *Phys.Rev.Lett.*, 87:122001, 2001.
- [51] V. Del Duca, W. Kilgore, C. Oleari, C. Schmidt, and D. Zeppenfeld. Gluon fusion contributions to H + 2 jet production. *Nucl.Phys.*, B616:367–399, 2001.
- [52] Francisco Campanario and Michael Kubocz. Higgs boson production in association with three jets via gluon fusion at the LHC: Gluonic contributions. *Phys.Rev.*, D88(5):054021, 2013.
- [53] H. van Deurzen, N. Greiner, G. Luisoni, P. Mastrolia, E. Mirabella, et al. NLO QCD corrections to the production of Higgs plus two jets at the LHC. *Phys.Lett.*, B721:74–81, 2013.
- [54] G. Cullen, H. van Deurzen, N. Greiner, G. Luisoni, P. Mastrolia, et al. Next-to-Leading-Order QCD Corrections to Higgs Boson Production Plus Three Jets in Gluon Fusion. *Phys.Rev.Lett.*, 111(13):131801, 2013.
- [55] Lance J. Dixon. Calculating scattering amplitudes efficiently. 1996.
- [56] Michael E. Peskin. Simplifying Multi-Jet QCD Computation. 2011.
- [57] W. Buchmuller and D. Wyler. Effective Lagrangian Analysis of New Interactions and Flavor Conservation. *Nucl.Phys.*, B268:621–653, 1986.
- [58] S. Dawson and R. Kauffman. QCD corrections to Higgs boson production: nonleading terms in the heavy quark limit. *Phys.Rev.*, D49:2298–2309, 1994.
- [59] J.A. Gracey. Classification and one loop renormalization of dimension-six and dimension-eight

- operators in quantum gluodynamics. *Nucl.Phys.*, B634:192–208, 2002.
- [60] Kirill Melnikov and Timo van Ritbergen. The Three loop relation between the MS-bar and the pole quark masses. *Phys.Lett.*, B482:99–108, 2000.
- [61] R.S. Pasechnik, O.V. Teryaev, and A. Szczurek. Scalar Higgs boson production in a fusion of two off-shell gluons. *Eur.Phys.J.*, C47:429–435, 2006.
- [62] John C. Collins, Frank Wilczek, and A. Zee. Low-Energy Manifestations of Heavy Particles: Application to the Neutral Current. *Phys.Rev.*, D18:242, 1978.
- [63] William B. Kilgore. One-Loop Single-Real-Emission Contributions to $pp \rightarrow H + X$ at Next-to-Next-to-Next-to-Leading Order. *Phys.Rev.*, D89:073008, 2014.
- [64] T. Gehrmann, M. Jaquier, E.W.N. Glover, and A. Koukoutsakis. Two-Loop QCD Corrections to the Helicity Amplitudes for $H \rightarrow 3$ partons. *JHEP*, 1202:056, 2012.
- [65] H. Kluberg-Stern and J.B. Zuber. Ward Identities and Some Clues to the Renormalization of Gauge Invariant Operators. *Phys.Rev.*, D12:467–481, 1975.
- [66] R. Tarrach. The Renormalization of Ff. *Nucl.Phys.*, B196:45, 1982.
- [67] Benjamin Grinstein and Lisa Randall. The Renormalization of g^2 . *Phys.Lett.*, B217:335, 1989.
- [68] L.F. Abbott. The Background Field Method Beyond One Loop. *Nucl.Phys.*, B185:189, 1981.
- [69] Adam Alloul, Neil D. Christensen, Cline Degrande, Claude Duhr, and Benjamin Fuks. FeynRules 2.0 - A complete toolbox for tree-level phenomenology. *Comput.Phys.Commun.*, 185:2250–2300, 2014.
- [70] Thomas Hahn. Generating Feynman diagrams and amplitudes with FeynArts 3. *Comput.Phys.Commun.*, 140:418–431, 2001.
- [71] T. Hahn and M. Perez-Victoria. Automatized one loop calculations in four-dimensions and D-dimensions. *Comput.Phys.Commun.*, 118:153–165, 1999.
- [72] R. Mertig, M. Bohm, and Ansgar Denner. FEYN CALC: Computer algebraic calculation of Feynman amplitudes. *Comput.Phys.Commun.*, 64:345–359, 1991.
- [73] R. Keith Ellis and Giulia Zanderighi. Scalar one-loop integrals for QCD. *JHEP*, 0802:002, 2008.
- [74] Carl R. Schmidt. $H \rightarrow ggg(gq\bar{q})$ at two loops in the large M_t limit. *Phys.Lett.*, B413:391–395, 1997.
- [75] B.W. Harris and J.F. Owens. The Two cutoff phase space slicing method. *Phys.Rev.*, D65:094032, 2002.

- [76] W. Beenakker, H. Kuijf, W.L. van Neerven, and J. Smith. QCD Corrections to Heavy Quark Production in p anti-p Collisions. *Phys.Rev.*, D40:54–82, 1989.
- [77] S. Dawson and R.P. Kauffman. Higgs boson plus multi - jet rates at the SSC. *Phys.Rev.Lett.*, 68:2273–2276, 1992.
- [78] Russel P. Kauffman, Satish V. Desai, and Dipesh Risal. Production of a Higgs boson plus two jets in hadronic collisions. *Phys.Rev.*, D55:4005–4015, 1997.
- [79] Lance J. Dixon and Yael Shadmi. Testing gluon self-interactions in three jet events at hadron colliders. *Nucl.Phys.*, B423:3–32, 1994.
- [80] Lance J. Dixon, E.W. Nigel Glover, and Valentin V. Khoze. MHV rules for Higgs plus multi-gluon amplitudes. *JHEP*, 0412:015, 2004.
- [81] Duff Neill. Analytic Virtual Corrections for Higgs Transverse Momentum Spectrum at $\mathcal{O}(\alpha_s^2/M_t^3)$ via Unitarity Methods. 2009.
- [82] Johannes Broedel and Lance J. Dixon. Color-kinematics duality and double-copy construction for amplitudes from higher-dimension operators. *JHEP*, 1210:091, 2012.
- [83] Freddy Cachazo, Peter Svrcek, and Edward Witten. MHV vertices and tree amplitudes in gauge theory. *JHEP*, 0409:006, 2004.
- [84] J. Alwall, R. Frederix, S. Frixione, V. Hirschi, F. Maltoni, et al. The automated computation of tree-level and next-to-leading order differential cross sections, and their matching to parton shower simulations. *JHEP*, 1407:079, 2014.
- [85] Celine Degrande, Claude Duhr, Benjamin Fuks, David Grellscheid, Olivier Mattelaer, et al. UFO - The Universal FeynRules Output. *Comput.Phys.Commun.*, 183:1201–1214, 2012.
- [86] J.F. Owens, A. Accardi, and W. Melnitchouk. Global parton distributions with nuclear and finite- Q^2 corrections. *Phys.Rev.*, D87(9):094012, 2013.
- [87] Daniel de Florian, Giancarlo Ferrera, Massimiliano Grazzini, and Damiano Tommasini. Transverse-momentum resummation: Higgs boson production at the Tevatron and the LHC. *JHEP*, 1111:064, 2011.

Appendix A: Virtual Contributions

Defining V_i , along with the logarithms and dilogarithms, as complex numbers, the one-loop qg virtual contributions proportional to C_1 are [74],

$$\begin{aligned}
V_1 &= -\frac{1}{\epsilon^2} \left[\left(\frac{m_H^2}{-S_{gq}} \right)^\epsilon + \left(\frac{m_H^2}{-S_{g\bar{q}}} \right)^\epsilon \right] + \frac{13}{6\epsilon} \left(\frac{m_H^2}{-S_{q\bar{q}}} \right)^\epsilon \\
&\quad - \log \left(\frac{S_{gq}}{m_H^2} \right) \log \left(\frac{S_{g\bar{q}}}{m_H^2} \right) - \log \left(\frac{S_{g\bar{q}}}{m_H^2} \right) \log \left(\frac{S_{q\bar{q}}}{m_H^2} \right) - 2Li_2 \left(1 - \frac{S_{q\bar{q}}}{m_H^2} \right) \\
&\quad - Li_2 \left(1 - \frac{S_{gq}}{m_H^2} \right) - Li_2 \left(1 - \frac{S_{g\bar{q}}}{m_H^2} \right) + \frac{40}{9} + \frac{\pi^2}{3} - \frac{S_{q\bar{q}}}{2S_{g\bar{q}}} \\
V_2 &= \left[\frac{1}{\epsilon^2} + \frac{3}{2\epsilon} \right] \left(\frac{m_H^2}{-S_{q\bar{q}}} \right)^\epsilon + \log \left(\frac{S_{gq}}{m_H^2} \right) \log \left(\frac{S_{g\bar{q}}}{m_H^2} \right) + Li_2 \left(1 - \frac{S_{gq}}{m_H^2} \right) \\
&\quad + Li_2 \left(1 - \frac{S_{g\bar{q}}}{m_H^2} \right) + 4 - \frac{\pi^2}{6} - \frac{S_{q\bar{q}}}{S_{g\bar{q}}} \\
V_3 &= -\frac{2}{3\epsilon} \left(\frac{m_H^2}{-S_{q\bar{q}}} \right)^\epsilon - \frac{10}{9}. \tag{A1}
\end{aligned}$$

These results are in agreement with Ref. [74]. The results must be analytically continued for timelike momentum invariants: $\log(S_{ij}) \rightarrow \log(|S_{ij}|) + i\pi\theta(-S_{ij})$ and $(-1)^\epsilon \rightarrow 1 + i\pi\epsilon - \frac{\epsilon^2\pi^2}{2}$.

The one-loop qg virtual contributions proportional to C_5 are (with W_i complex),

$$\begin{aligned}
W_1 &= \frac{1}{\epsilon^2} \left[\left(\frac{m_H^2}{-S_{g\bar{q}}} \right)^\epsilon + \left(\frac{m_H^2}{-S_{gq}} \right)^\epsilon \right] + \frac{1}{\epsilon} \left[\frac{17}{6} \right] \\
&\quad - \log \left(\frac{S_{gq}}{m_H^2} \right) - \frac{33}{18} \log \left(\frac{S_{g\bar{q}}}{m_H^2} \right) + \frac{121}{18} + \frac{1}{6} \frac{S_{g\bar{q}}}{S_{gq}} + \frac{1}{3} \frac{S_{q\bar{q}}}{S_{gq}} \\
W_2 &= -\frac{1}{\epsilon^2} \left(\frac{m_H^2}{-S_{q\bar{q}}} \right)^\epsilon + \frac{1}{\epsilon} \left[-\frac{17}{6} \right] + \log \left(\frac{S_{gq}}{m_H^2} \right) + \frac{1}{3} \log \left(\frac{S_{g\bar{q}}}{m_H^2} \right) \\
&\quad + \frac{3}{2} \log \left(\frac{S_{q\bar{q}}}{m_H^2} \right) - \frac{103}{18} + \frac{1}{3} \frac{S_{g\bar{q}}}{S_{gq}} + \frac{1}{6} \frac{S_{q\bar{q}}}{S_{gq}} \tag{A2}
\end{aligned}$$

$$W_3 = \frac{2}{3} \left[\frac{1}{\epsilon} - \log \left(\frac{-S_{q\bar{q}}}{m_H^2} \right) \right] + \frac{10}{9}. \tag{A3}$$

This result is in disagreement with that of Ref. [81].

The one-loop gg contribution proportional to C_1 is,

$$\begin{aligned}
U_1 &= -\frac{1}{\epsilon^2} \left[\left(\frac{m_H^2}{-S_{12}} \right)^\epsilon + \left(\frac{m_H^2}{-S_{23}} \right)^\epsilon + \left(\frac{m_H^2}{-S_{31}} \right)^\epsilon \right] \\
&\quad - \log \left(\frac{S_{23}}{m_H^2} \right) \log \left(\frac{S_{31}}{m_H^2} \right) - \log \left(\frac{S_{31}}{m_H^2} \right) \log \left(\frac{S_{12}}{m_H^2} \right) \\
&\quad - \log \left(\frac{S_{12}}{m_H^2} \right) \log \left(\frac{S_{23}}{m_H^2} \right) - 2Li_2 \left(1 - \frac{S_{12}}{m_H^2} \right) \\
&\quad - 2Li_2 \left(1 - \frac{S_{23}}{m_H^2} \right) - 2Li_2 \left(1 - \frac{S_{31}}{m_H^2} \right),
\end{aligned}$$

which agrees with Eq. (11) of Ref. [74].

The one-loop gg contribution proportional to C_3 is,

$$U_3 = -\frac{3}{\epsilon^2(1-2\epsilon)} \left[\left(\frac{m_H^2}{-S_{12}} \right)^\epsilon + \left(\frac{m_H^2}{-S_{23}} \right)^\epsilon + \left(\frac{m_H^2}{-S_{31}} \right)^\epsilon \right] + O(\epsilon). \quad (\text{A4})$$

Appendix B: NLO Real Emission - Quark Amplitudes

1. $q\bar{q}ggh$ amplitudes

The contribution from O_3 , to be multiplied by C_3 , is

$$im^{O_3}(q_-(1), g_-(2), g_-(3), \bar{q}_+(4), h) = -3ig_s \frac{\langle 12 \rangle \langle 23 \rangle \langle 31 \rangle}{\langle 14 \rangle}, \quad (\text{B1})$$

$$im^{O_3}(q_-(1), g_-(2), g_+(3), \bar{q}_+(4), h) = 0, \quad (\text{B2})$$

$$im^{O_3}(q_-(1), g_+(2), g_-(3), \bar{q}_+(4), h) = 0, \quad (\text{B3})$$

$$(\text{B4})$$

Just like the $ggggh$ amplitudes in Section VI, Eq. (B2) demonstrates non-interference with the O_1 amplitude in the soft Higgs limit. The O_4 operator contains two pairs of quark bilinears, so does not contribute to the $q\bar{q}ggh$ tree amplitude. The O_5 operator is easily shown to satisfy the operator relation

$$O_5 = O_4 + \partial^\alpha h G_{\alpha\nu}^A D^\beta G_\beta^{A\nu}, \quad (\text{B5})$$

up to total derivatives, which leads to the following contributions proportional to p_H , to be multiplied by C_5 ,

$$im^{O_5}(q_-(1), g_+(2), g_-(3), \bar{q}_+(4), h) = g_s^2 \left[\frac{i\langle 13 \rangle \langle 3\cancel{p}_H 2 \rangle \langle 1\cancel{p}_H 4 \rangle}{2\langle 12 \rangle S_{23}} - \frac{i[24] \langle 1\cancel{p}_H 2 \rangle \langle 1\cancel{p}_H 4 \rangle}{2\langle 12 \rangle [23][34]} + \frac{i[24] \langle 13 \rangle^2}{\langle 12 \rangle S_{23}} p_H \cdot (p_2 + p_3) \right], \quad (\text{B6})$$

$$im^{O_5}(q_-(1), g_-(2), g_+(3), \bar{q}_+(4), h) = g_s^2 \left[\frac{i\langle 12 \rangle [34]}{S_{23}[12]\langle 34 \rangle} ([13]\langle 34 \rangle p_H \cdot p_3 - [12]\langle 24 \rangle p_H \cdot p_2) - \frac{i\langle 2\cancel{p}_H 3 \rangle}{2\langle 34 \rangle [12] S_{23}} (S_{13}S_{34} - S_{24}S_{12} + S_{23}S_{34} - S_{23}S_{12}) \right], \quad (\text{B7})$$

$$im^{O_5}(q_-(1), g_-(2), g_-(3), \bar{q}_+(4), h) = g_s^2 \left[-\frac{i(S_{12} + S_{13} + S_{23})\langle 3\cancel{p}_H 4 \rangle}{2[12][23]} - \frac{i\langle 1\cancel{p}_H 4 \rangle \langle 2\cancel{p}_H 4 \rangle}{2[23][34]} \right] \quad (\text{B8})$$

2. $q\bar{q}q\bar{q}$ and $q\bar{q}Q\bar{Q}$ amplitudes

The O_3 amplitude vanishes at tree-level due to the absence of the ggh vertex. For O_4 and O_5 , we define

$$f_4(p_1, p_2, p_3, p_4) = 2i\langle 14 \rangle [32], \quad (\text{B9})$$

$$f_5(p_1, p_2, p_3, p_4) = \frac{i}{2} \left(\frac{1}{S_{12}} + \frac{1}{S_{34}} \right) \left[\langle 1\cancel{p}_H 2 \rangle \langle 4\cancel{p}_H 3 \rangle + \langle 14 \rangle [23] (p_1 + p_2) \cdot (p_3 + p_4) \right]. \quad (\text{B10})$$

The amplitudes for O_i , $i = 4, 5$, are

$$\begin{aligned} im^{O_i} (q_-^{c_1}(1), \bar{q}_+^{c_2}(2), Q_+^{c_3}(3), \bar{Q}_-^{c_4}, h) &= im^{O_i} (q_-^{c_1}(1), \bar{q}_+^{c_2}(2), q_+^{c_3}(3), \bar{q}_-^{c_4}, h) \\ &= g_s^2 f_i(p_1, p_2, p_3, p_4) \sum_A T_{c_1 c_2}^A T_{c_3 c_4}^A, \end{aligned} \quad (\text{B11})$$

$$\begin{aligned} im^{O_i} (q_-^{c_1}(1), \bar{q}_+^{c_2}(2), q_-^{c_3}(3), \bar{q}_+^{c_4}, h) &= g_s^2 f_i(p_1, p_2, p_4, p_3) \sum_A T_{c_1 c_2}^A T_{c_3 c_4}^A, \\ &+ f_i(p_3, p_2, p_4, p_1) \sum_A T_{c_3 c_2}^A T_{c_1 c_4}^A, \end{aligned} \quad (\text{B12})$$

where q and Q represent different flavor quarks.